 doi:10.20944/preprints202206.0061.v1

*Article*

# On Wire-Grid Representation for Modeling Symmetrical Antenna Elements

**Adnan Alhaj Hasan [1]*, Dmitriy V. Klyukin [1], Aleksey A. Kvasnikov [1], Maxim E. Komnatnov [1] and Sergei P. Kuksenko [1]**

[1] Scientific Research Laboratory of Basic Research on Electromagnetic Compatibility, Tomsk State University of Control Systems and Radioelectronics, 634050 Tomsk, Russia; alhaj.hasan.adnan@tu.tusur.ru (A.A.H); dv_klyukin@tu.tusur.ru (D.V.K.); aleksejkvasnikov@tu.tusur.ru (A.A.K.); maxmek@mail.ru (M.E.K.); ksergp@tu.tusur.ru (S.P.K.).

* Correspondence: alhaj.hasan.adnan@tu.tusur.ru.

**Abstract:** This paper focuses on the combination of the method of moments and the wire-grid approximation as an effective computational technique for modeling symmetrical antennas with low computational cost and quite accurate results. The criteria and conditions for the use of wire-grid surface approximation from various sources are presented together with new recommendations for modeling symmetrical antenna structures using the wire-grid approximation. These recommendations are used to calculate the characteristics of biconical and horn antennas at different frequencies. The results obtained using different grid and mesh settings are compared to those obtained analytically. Moreover, the results are compared to those obtained using the finite difference time domain numerical method, as well as the measured ones. All results are shown to be in a good agreement. The used recommendations for building a symmetrical wire-grid of those symmetrical antenna elements provided the most advantageous parameters of the grid and mesh settings and the wire radius, which are able to give a quite accurate results with low computational cost. Additionally, the known equal area rule was modified for a rectangular grid form. The obtained radiation patterns of a conductive plate using both the original rule and the modified one are compared with the electrodynamic analysis results. It is shown that the use of the modified rule is more accurate when using a rectangle grid form.

**Keywords:** computational electromagnetics; numerical methods; method of moments; antennas; radiation pattern; input impedance; simulation software

## 1. Introduction

The importance of designing new antenna elements (AE) is increasing since they have a significant impact on the radio electronic systems rapid development. The demand on using the digital active phased array antennas is also remarkably arising from the challenge in designing and manufacturing such antennas to meet the expectations which include but not limited to: high quality, low cost and reliable final product. Nowadays, various computer-aided design (CAD) systems are used to estimate the effectiveness of the proposed technical solutions and adjust them if necessary. CAD is based on the numerical solution of Maxwell's equations or their derivatives, since analytical solutions are known only for particular AEs. The use of CAD allows researchers to significantly reduce the time of AE development, optimize their characteristics, as well as reduce the financial costs of design. Meanwhile, each numerical method of computational electrodynamics has its own field of application, where they are most effective. Nevertheless, despite the achieved successes in the development of specialized CAD systems and numerical methods, it is currently unknown whether a universal numerical method suitable for solving all problems of electrodynamics can be created [1]. Consequently, one of the main challenges in solving electrodynamic problems is to choose the "optimal" method (calculation

 doi:10.20944/preprints202206.0061.v1



method) for solving a specific problem. According to [2], "the method is called optimal for solving a given class of problems with the required accuracy on a specified computing system if it allows you to get a result with minimal resource costs." Currently, there are many popular methods to solve electrodynamic problems numerically. The finite difference method in the time domain (FDTD), was first described by K. Yee in 1966 [3], and the abbreviation of its name was proposed by A. Taflove [4]. The finite integration method (FIT) was proposed by T. Weiland in 1977 as a computational tool for solving Maxwell's equations [5]. The method can be implemented in both time and frequency domains. FDTD can be considered to be a special case of the FIT [6]. The finite element method (FEM) is widely used in the mechanical analysis of structures. Despite the fact that the mathematical interpretation of the method was proposed in 1943 by Courant [7], it was not used to solve electromagnetic problems until 1968. In general, these methods can solve problems of a complex structure and give accurate results. However, this happens at the expense of computational cost, especially when solving electrodynamic problems in the frequency domain, what will dramatically increase the costs to achieve the same required accuracy. The method of moments (MoM) seems to be most promising and more efficient for solving AE problems at relatively low computing costs. In relation to electrodynamic problems, the use of the MoM provides the following stages of solution. First, the metal parts of the studied AE are replaced by equivalent surface electric currents. Appropriate boundary conditions are imposed on the resulting solution of the metal elements to calculate the equivalent currents. Then, the problem of exciting the environment with these currents is solved. An important aspect of such process is the discretization of the metal surfaces into elementary areas and the approximation of the current within each such area.

To approximate the curved boundaries of surfaces of an arbitrary shape, it is common to use the discretization into triangles, and to represent the current in them, using the vector basic functions RWG (Rao, Wilton, Glisson) [8]. This approach may be computationally costly because of the time and memory required to build the numerical mesh and also the increase in the costs due to the need to solve a problem with the obtained big mesh. Moreover, the obtained mesh is not symmetrical, and it is sometimes hard to adjust it. Since the surface current in the symmetrical AE structures seems to distribute symmetrically through the structure in a narrow frequency range, its more logical to get a symmetrical mesh for a symmetrical structure. Therefore, this approach may not be efficient.

As is known, the analysis of wire linear AEs is reduced to solving the integral Pocklington [9] and Hallen [10] equations. The features of the solution of these equations are based on the thin-wire approximation [11–18]. In this approach, the wire is assumed to be an ideal conductor in the form of a cylinder located along one of the coordinate axes (a one-dimensional problem), with a radius much smaller than the wavelength of the excitation signal and the cylinder physical length. This simplification enables using a scalar current density function instead of a vector one, which greatly simplifies the complexity of the task. This approach is also applicable to the representation the AE surfaces by a wire-grid [19]. Such approach in combination with formulations of integral equations of the electric field and the MoM is widely used in well-known software products such as NEC [20]. Although, in comparison with the surface triangular approximation and the use of RWG functions, this approach demonstrates its inherent weaknesses in near-field analysis, it has proven its efficiency on a large number of far-field scattering and radiation problems associated with conducting bodies of an arbitrary shape [21–25]. Therefore, the wire-grid approximation continues to be widely used in computational electrodynamics [26, 27], since it is very easy to adjust the obtained grid and it is more suitable for building a symmetrical grid for symmetrical structures.

There are many studies on summarizing and forming the criteria and conditions for the use of wire-grid surface approximation for AE modeling [19, 20, 23, 28–31]. In these sources, the proposed recommendations are not suitable for any AE structure and depend on the used weight and basics functions.

 doi:10.20944/preprints202206.0061.v1



This work is aimed to propose new recommendations for modeling symmetrical AE structures using the wire-grid surface approximation approach in combination with MoM.

## 2. Materials and Methods

None of the existing numerical methods is suitable for all electrodynamic modeling problems. Thus, MoM program codes are practically unsuitable for describing inhomogeneous nonlinear dielectrics. FEM codes cannot effectively solve large scattering problems. Unfortunately, there are tasks where it is necessary to take into account all these features, for example, when evaluating radiation from a printed circuit board, and therefore, the analysis cannot be performed by any of these methods. One of the solutions to this problem is to combine two or more methods in one program code. In this case, one of the methods is often MoM [32–39]. Each method is applied to the task field for which it is best suited. Appropriate boundary conditions are applied at the interfaces between these fields. Separately, it should be noted that the FDTD, FEM, and MoM are the most universal methods and the largest number of books are devoted to their consideration where these methods are considered together, for example [1, 40–43]. The choice of a particular numerical method is based on the use of some criteria: the complexity of the geometry of the analyzed object; its electrical dimensions; available computing power; etc.

Using MoM has an advantage since the modeled object can have a complex shape. In addition, MoM is most effective for open geometries with linear and homogeneous media. The method is excellent for hybridization with other methods and asymptotic procedures, for example, FMM and MLFMM (fast multipole method and multilevel fast multipole method), as well as UTD and GTD (homogeneous and geometric diffraction theory) [44]. Unlike FEM and FDTD methods, MoM, when constructing the grid, does not require discretization of the volume, in which the analyzed object is enclosed. It only requires discretization of the surface of this object, which gives a relatively small cost for this procedure. Similarly to any other method, MOM has a disadvantages, in particular, it is difficult to model internal problems and heterogeneous media with this method. Besides, the calculation speed is sometimes low for objects of a relatively simple shape. However, this is easily eliminated by the speed increasing of workstations and developing of numerical procedures, which makes it possible to speed up the overall solution process using MoM [45].

Based on the above, to solve antenna problems, it seems most effective to use the MoM, which is "surface" and not "volumetric" like the others, since its use does not require the boundary conditions that emulate remote boundaries to be artificially set. This reduces the dimension of the problem, reducing, for example, a three-dimensional problem to a two-dimensional one. In addition, the method allows for hybridization with other numerical methods. Therefore, if necessary, the functionality of the software module can be significantly expanded in the future. The computational aspects of MoM are considered in detail in [46–49].

When using a particular numerical method, the important issue is related to its convergence rate and the accuracy of the results obtained with its help. Convergence when using MoM directly depends on the operator, the basis and test functions, as well as their number. At the same time, the effectiveness of using the method to obtain a result with a given accuracy is determined by the computational costs (the time and the memory of the workstation used). As a result, when calculating by the method of moments, an unknown quantity (for example, a field or current density) depending on spatial coordinates is approximated by a finite number of known functions (called basis functions) multiplied by unknown coefficients. This approximation is substituted into a linear operator equation. The left and right sides of the resulting equation are multiplied by a suitable function (called a test or weight function) and integrated over the domain in which the test function is defined. Then the linear operator equation reduces to a system of linear algebraic equation (SLAE). Repeating this procedure for a set of independent test functions, the number

Preprints (www.preprints.org) | NOT PEER-REVIEWED | Posted: 6 June 2022 doi:10.20944/preprints202206.0061.v1



of which should be equal to the number of basic functions, SLAEs are obtained. SLAEs solution gives unknown coefficients and allows finding an approximate solution to the operator equation. Further, the characteristics of interest are determined from the SLAEs solution.

The MoM is widely applicable in modeling antennas of various classes. In addition, the method is most effective if the AE contains only perfectly conductive elements. In MoM, the choice of basic and test functions is determined by the shape of the entire conductive surface (structure). The most commonly used basic functions are called the piecewise functions. They have a constant value in each meshing cell and equal to zero outside of it [50, 51]. One of the frequently used test functions that are not used as basic ones are Dirac delta functions (single impulse functions. When both piecewise and Dirac delta functions are employed, the MoM is known as the collocation method [52]. In addition, when similar basic and testing functions are employed, the MoM is known as the Galerkin method [47, 48].

As mentioned above, an important aspect of using the MoM is the discretization of metal surfaces into elementary areas and the approximation of the current within each such area. Therefore, a summary of the recommendations for criteria and conditions, extracted from various sources, can be formulated for the use of wire-grid surface approximation in AE modeling [19, 20, 23, 28–31]:

1. The assumption of a thin wire must be fulfilled, i.e., the length of the wire $L$ and the wavelength $\lambda$ must be much larger than its radius $a$;
2. The wires of the grid should not intersect with each other along the length without forming a node (Figure 1). Hence, if two wires are electrically connected at their ends, then for current interpolation it is necessary to use the same coordinates to specify these ends;

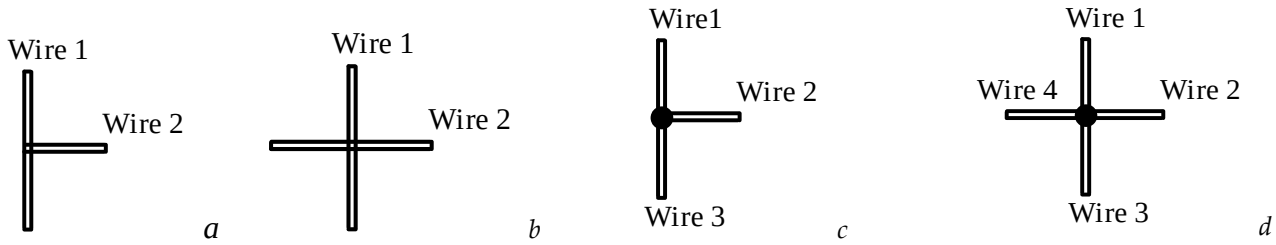


Figure 1. Incorrect (*a*, *b*) and correct wire intersections (*c*, *d*)

3. Parallel wires should not be too close to each other. Hence, the distance between the axis of two (or more) wires connected in parallel should exceed their largest radius by more than 4 times;
4. The minimum number of basic functions for electrically shorted wires should be 3, especially if they are part of a wire-grid. For electrically short AEs, this number should be 8-10;
5. For an electrically short dipole, the number of segments (basic functions) must be at least 12-16;
6. For each individual wire, it is necessary to separately set the number of segments (basic functions) based on the frequency of the excitation signal (single calculation) or the highest frequency if the wire is modeled in the frequency range (multiple calculations). At the same time, it is not recommended to use less than 8-10 segments;
7. When setting the excitation at the intersection of the wires, an additional wire consisting of three segments is used. The source is set in the central part of this wire (Figure 2). In this case, all segments in contact with the segment where the excitation source is located and near it must have the same length;

Preprints (www.preprints.org) | NOT PEER-REVIEWED | Posted: 6 June 2022 doi:10.20944/preprints202206.0061.v1



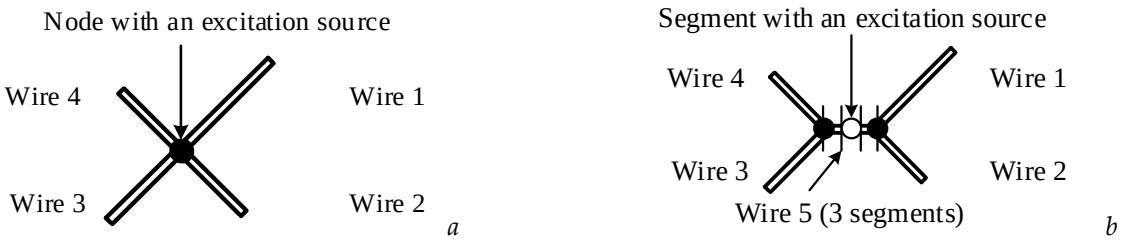


Figure 2. Incorrect (*a*) and correct (*b*) setting of the excitation source at the wire intersection

8. In most cases, the length of the segments should be less than λ / 10, and when describing complex geometric transitions – λ / 20. For large extended wire sections, the length of the segments can be increased, but it should not be less than λ / 5. At the same time, you should avoid using very short segments with a length of less than 0.0001 λ;
9. In most cases, the length of the segments should be more than 8–10 times their radius;
10. In most cases, the appropriate wire-grid mesh is λ / 10 for the middle of the frequency range;
11. The radius of the wire when using a wire-grid is determined through the surface area of the wires (the equivalent area rule). Thus, Figure 3 shows a grid element with a size of Δ × Δ formed by four wires, and the surface area of a wire with a diameter of 2*a*. As a result, with a known grid step Δ, the required wire radius is defined as [53]

$$a = \Delta/2\pi. \quad (1)$$

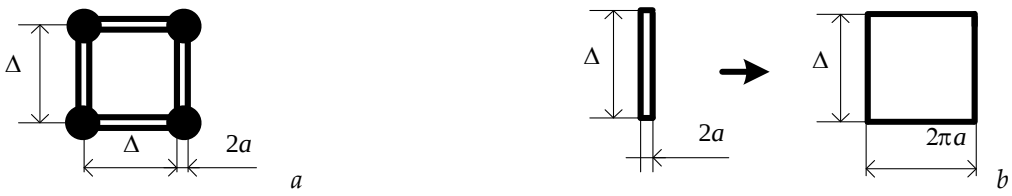


Figure 3. A wire-gird element (*a*) and the area of one wire surface (*b*)

12. If the wire-grid covers a surface having an irregular shape, then the equivalent area rule can be generalized as in [31]. Figure 4 shows an example of an approximation of a curved surface consisting of two regions *A*1 and *A*2. The required wire radius is calculated as

$$a = (A_1+A_2)/4\Delta\pi. \quad (2)$$

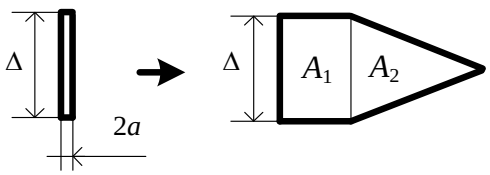


Figure 4. Modeling a curved surface with a single wire

Using the above recommendations is not enough, and there are some problems occurring during the modeling process. In what follows, some cases will be presented in

Preprints (www.preprints.org) | NOT PEER-REVIEWED | Posted: 6 June 2022 doi:10.20944/preprints202206.0061.v1



which considering the traditional recommendations for modeling symmetrical AE structures using wire-grid approximation does not give correct results, and it is necessary to adjust these recommendations to get appropriate results. Moreover, some recommendations will be presented for modeling such structures, and the results will be validated by comparing them with those obtained analytically and experimentally, as well as numerically with another method. To do this and based on the wire-grid approximation and the MoM, a program module was developed using C++ programming language with OpenMP, VTK library, and the QT cross-platform software. This module (furtheron referred to as the wire-grid) is used to calculate all the obtained results in this work. Besides, the Octave mathematical package was used to estimate the software implementation of the analytical models used later in this work to validate the results obtained using the wire-grid.

## 3. Problems, solutions and results

### *3.1. Modeling of a monopole on plate using wire-grid*

In the MoM, when wires are used to split the surfaces of the conductive parts in the structure into elementary platforms and approximate the current within them, a scalar current density function is used instead of a vector function, which greatly simplifies the solution. In this case, a preliminary choice of the number of the wires and their radius is required. The equal area rule is typically employed for constructing a square grid of wires when solving scattering problems [23, 26, 31, 54, 55]. However, the construction of such a grid is not always feasible, so it is necessary to use a different grid. Thus, we present a simple modification of the equal area rule for modeling structures using the wire-grid when solving the radiation problem.

The known equal area rule is based on replacing a square polygon with a grid of wires, the radii of which are based on the size of the polygon [26]. The influence of the wire-grid size constructed considering this rule on the accuracy of the obtained results is investigated in [54]. The rule is generalized to the case of approximation of a surface consisting of square and triangular polygons [31]. The physical interpretation of the equal area rule is given in [55]. According to this rule, to approximate a square polygon with a separate wire, its radius $a$ is determined so that the surface areas of the polygon and a wire length $\Delta$ coincide as in (1) (see Figure 5*a*) [26].

However, this rule cannot be applied in the case of a rectangular grid. In this case, it is proposed to use the length of the smaller side of the rectangle $\Delta_2$ (Figure 5*b*), i.e.

$$a = \Delta_2 / 2\pi. \tag{3}$$

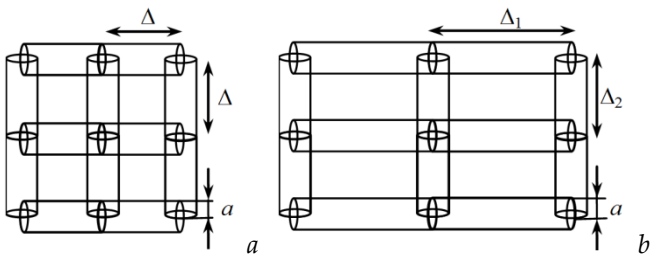


Figure 5. Demonstration of the equal area rule [26] (*a*) and its modification (*b*)

Testing was performed on the example of a dipole oriented along the $x$ axis on a conducting plate 25×50 mm² located in the $yz$ plane. The dipole with a length of 12.5 mm (the length of its shoulders was 5, and the gap was 2.5 mm) and a radius of 0.015 mm was located at a distance of $\lambda/4$ from the end of the plate. The excitation frequency was 7.56 GHz ($\lambda \approx 39.655$ mm). The wires with the radii calculated by (1) and (3) were modeled

Preprints (www.preprints.org) | NOT PEER-REVIEWED | Posted: 6 June 2022 doi:10.20944/preprints202206.0061.v1



using the wire-grid approximation. The EMPro (FDTD) system [56] was used for verification. The excitation port had the following characteristics: the amplitude of 1 V; the internal resistance of 0 ohms; the signal form was "broadband". The segment length in both systems was assumed to be λ/10. Using the wire-grid approximation, the plate was approximated by a grid $L_y \times L_z$ where $L_y$ and $L_z$ are the step numbers of the grid along the $y$ and $z$ axes. When a square grid was used, these values were assumed to be 8 and 4, respectively (the lengths of the wire segments on both axes were 6.25 mm). According to (1), the radius of the wires $a$ =0.9947 mm was obtained. At λ/10, the length of the segments was 3.125 mm, which satisfies the conditions in the recommendation 1 and 10 (later will be referred to as conditions (1, 10) ). As a result, each piece of wire was divided into 2 segments. The total number of segments $N$ was 157. When a rectangular grid was used, $L_y=L_z=8$ was assumed (the lengths of the wire segments along the $y$ and $z$ axes were 6.25 and 3.125 mm). The radius of the wires according to (3) was 0.5 mm, and the length of the segments was 3.125 mm, which also satisfies the conditions (1, 10). The wire segments along the $y$ axis were divided into 2 segments, and $z$ were not divided and the value of $N$ was 221. The obtained radiation patterns (RP) are shown in Figure 6, and at θ=0, 1, ..., 180, φ = 0°, 45° and 90° – in Figure 7.

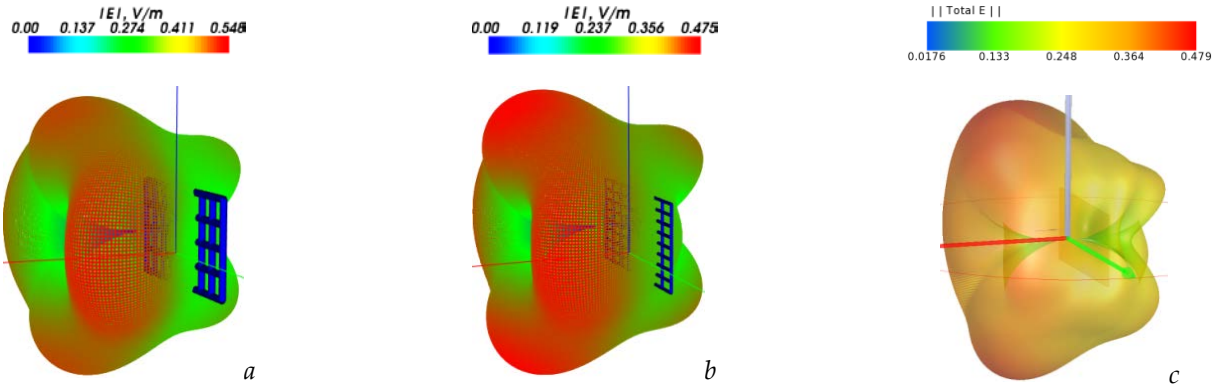


Figure 6.The RP of a dipole on a conducting plate modeled using the wire-grid by (1) (*a*), by (3) (*b*) and EMPro (*c*)

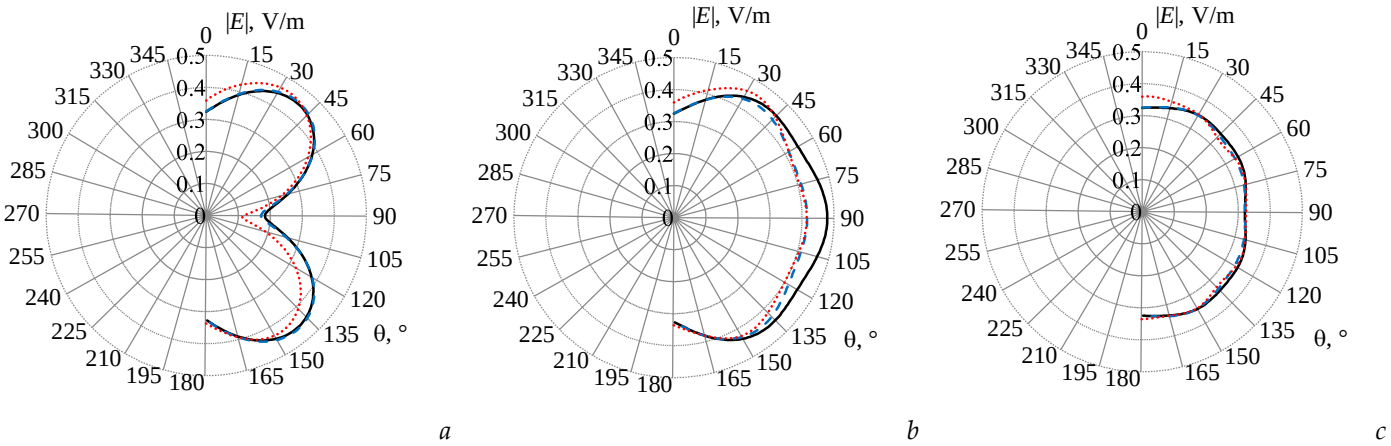


Figure 7. The RP of a dipole on a conducting plate at θ = 0, 1, ..., 180°, φ = 0° (*a*), 45° (*b*) and 90° (*c*) using the wire-grid by (1) (—), by (3) (----), and EMPro (····)

From Figures 6 and 7 it can be seen that the results of EMPro and with the wire-grid by (3) agree very well, and the maximum of the electric field strength magnitudes $|E|$ are

Preprints (www.preprints.org) | NOT PEER-REVIEWED | Posted: 6 June 2022 doi:10.20944/preprints202206.0061.v1



very close: 0.479 and 0.475 V/m (the difference is less than 1%). When using (1), the maximum $|E|$ was 0.548 V/m (13% difference from EMPro). Thus, one can say that the proposed rule (3) gives more accurate results compared to (1).

### *3.2. Modeling symmetrical biconical AEs*

When modeling a complex structure, like a symmetrical biconical AE presented in (Figure 8), it is inappropriate to use the traditional recommendations for modeling. The number of wires and their radii are difficult to determine, as well as the radius of the wire where the excitation source is located. Moreover, to answer the questions about wire location in the grid (horizontal and vertical grid elements) and the effect of the segment step on the results is not a trivial issue here. Therefore, the following model-testing based on wire-grid approximation model was performed in order to reveal an optimal setting for modeling such AE structure.

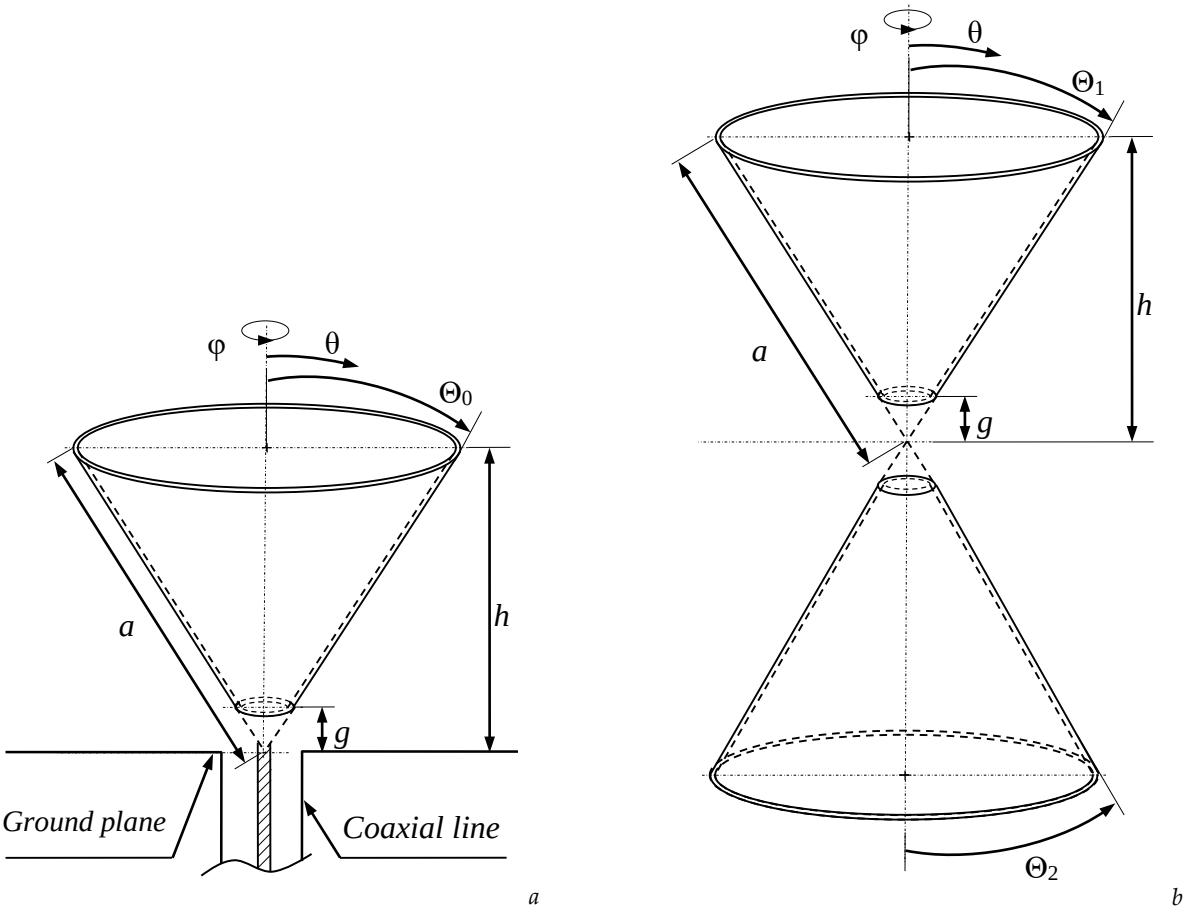


Figure 8. The conical (*a*) and the biconical (*b*) AEs

When the wire-grid approximation was employed based on the convergence of the results obtained by increasing the number of wires (4, 8, 16, 32, 64, and 128) approximating the AE surface, it was found that their optimal number is 64. The horizontal grid elements were not used here because the amplitudes of the distributed currents among them are very small and their contribution to the radiated electric field is negligible. The values of the length of the segment $l_s$, the radius of the structure wires $a_s$ and the radius of the wire in the gap (excitation source) $a_{gap}$, were determined as $l_s = \lambda / n$, $a_s = l_s / 10$, $a_{gap} = l_s / 5$, respectively. The wire in the gap was approximated by one segment. A general view of the biconical AE at specified frequencies is shown in Figure 9.

Preprints (www.preprints.org) | NOT PEER-REVIEWED | Posted: 6 June 2022 doi:10.20944/preprints202206.0061.v1



Calculations of the radiotechnical characteristics (RTC) of the biconical AE were performed using the wire-grid, as well as the EMPro at frequencies of 0.1, 0.5, and 1 GHz with a gap length of 20 mm. The obtained results are compared to each other and to those obtained using well–known analytical expressions [57–59] (see Appendix A) to verify them and to prove that the proposed recommendations can give accurate results with low computational costs.

In general, the resulting inaccurate solution is not necessarily related to the used computational algorithm of the numerical method that was employed; it may be related to the solved mathematical problem itself. Even with an accurate calculation, the solution of the problem can be very sensitive to the disturbances in the input data. The qualitative concept of this sensitivity and its quantitative measure, which is called conditionality, are related to the influence of the disturbances in the input data on the resulting solution. Therefore, a problem is called insensitive or well-conditioned if this relative change in the input data causes a reasonably commensurate relative change in the solution. On the contrary, task is considered sensitive or poorly conditioned if the relative change in the solution can be much greater than it is in the input data. For quantitative evaluation, the condition number of the problem is used in the form of the ratio of the relative change in the solution to the relative change in the input data. Then, the task is poorly conditioned or sensitive if its condition number is much greater than one. Otherwise, the task is considered well-conditioned.

Since the MoM reduces the surface integral equation of the electric field to a SLAE, which integrally contains all the information about the object under study, the properties of the obtained SLAE have to be analyzed in order to assess the stability of the problem solution; in the case under consideration – RTC AE. Therefore, when using MoM, many elements of matrix **Z** and of vectors **V** are obtained by numerical integration. Consequently, small errors in integration can be "increased" by a poorly conditioned **Z** matrix. In general, it is customary to evaluate the measure of conditionality of a matrix using its condition number [60]

$$\mathrm{cond}(Z)=||Z||\,||Z^{-1}|| \tag{4}$$

where $||\cdot||$ is a certain matrix norm. Conditionality characterizes the sensitivity of the SLAE solution to the changes in the values of the matrix elements. The higher the condition number of the matrix, the worse it is conditioned (for a single element matrix it is equal to 1). As the condition number of increases, the error of the solution increases because floating-point numbers are represented by a finite number of digits [61]. One of the important consequences of this is that a correct solution of SLAE cannot be obtained by the Gauss method with a small bit representation of numbers because of the large condition number of matrix **Z** [62]. As a result, the required numerical accuracy of the calculated result must exceed the probable number of the lost digits since the errors are rounded during calculations. This number of digits can be estimated by the conditionality number of the matrix. So, basically, if $\mathrm{cond}(\mathbf{Z}) = O(10^p)$ and the source data have an error in the $k^{\text{th}}$ decimal point, then regardless of the used method for solving the SLAE equation $\mathbf{ZI} = \mathbf{V}$, it is guaranteed to get its solution with no more than $k - p$ decimal points [63].

For example, suppose that when the convergence of a solution is investigated by increasing the number of basic functions, the condition number of matrix **Z** is of the order of $10^6$. Then, if it is necessary that the results for the input impedance converge to the fifth decimal point, then the elements of the matrix **Z** must be calculated with an accuracy of at least 11 digits, and this number of digits must be preserved in all calculations [63]. Remember that the condition number does not give an exact value of the maximum error of the method used, but only allows estimating its order. Therefore, you can specify an upper bound for the condition number, if it is exceeded, the solution of the SLAE at a particular workstation will lead to false results. Thus, if

$$\mathrm{cond}(\mathbf{Z}) \geq 1/eps \tag{5}$$

Preprints (www.preprints.org) | NOT PEER-REVIEWED | Posted: 6 June 2022 doi:10.20944/preprints202206.0061.v1



where *eps* is the machine epsilon, then the solution is considered unreliable [61, 63, 64].

According to IEEE 754–2008, for calculations with single and double precision, the *eps* value is $O(10^{-7})$ and $O(10^{-16})$, respectively. Often, when solving large-scale problems, even the conditionality number of matrix **Z** is large, but it is less than 1 / *eps*, so the MoM is workable [65]. However, the conditionality of the SLAE matrix worsens when the excitation frequency approaches the frequencies of natural oscillations (internal resonances) of the structure under study, especially at low frequencies [65]. Since the excitation frequency is selected discretely, there is a possibility of such a coincidence. The solution at this frequency may not be obtained at all, and at close frequencies it may be inaccurate or completely incorrect. For example, [66–70] are devoted to demonstrating the presence of imaginary resonances that do not exist in reality. To avoid this, it's necessary to increase the bit depth of the number representation [71] or to use the iterative methods [62, 72].

The influence of the mesh step (segments), set as $\lambda / n$, on the accuracy of the calculated RTC of AEs at $n = 10$, 20, and 40 was studied. The required orders of the formed matrices **Z** of the SLAE and their condition number (*cond*) calculated by (4) when using the wire-grid are summarized in Table 1.

The values of the input impedance of the biconical AE obtained using the wire-grid and the EMPro (FDTD) system, are summarized in Table 2. The table shows that the results obtained in the developed wire-grid software, as well as the EMPro (FDTD) system, converge when the grid step decreases. Table 4 shows the deviations of the input impedance magnitude values obtained in EMPro and using the wire-grid, relative to those obtained by analytical expressions. It can be seen that reducing the grid step gives values closer to the analytical ones, and using the wire-grid approximation gives closer results to the analytical ones from EMPro with less computational costs. In the EMPro system at $n = 40$, no results were obtained, due to machine memory limitations, so they are not listed in the tables (marked as «–»). The elapsed simulation time (*T*) and the used memory (*M*) for simulating the RTC of the of the biconical AE using the wire-grid and EMPro, are presented in Table 4 and Table 5, respectively.

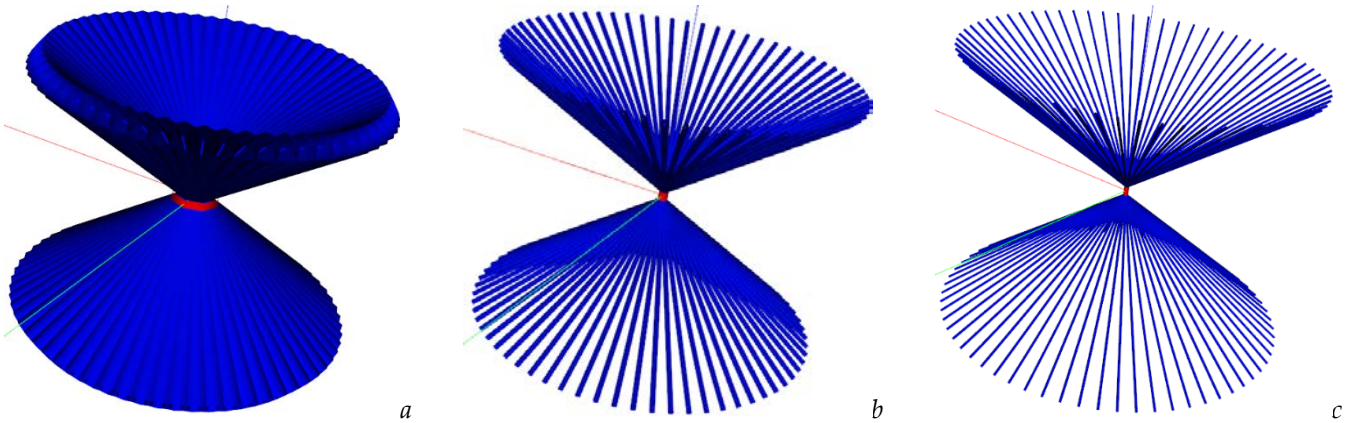

*a* *b* *c*

Figure 9. A general view of the biconical AE at frequencies of 0.1 (*a*), 0.5 (*b*), and 1 GHz (*c*) (the view is changing because the wire radius reduces with the frequency growth)

Preprints (www.preprints.org) | NOT PEER-REVIEWED | Posted: 6 June 2022 doi:10.20944/preprints202206.0061.v1



**Table 1**. The matrix **Z** orders *N* and their condition numbers, for the biconical AE with $a$ = 508 mm and $\Theta_1 = \Theta_2 = 53.1°$at frequencies of 0.1, 0.2 and 1 GHz and mesh step (segment size) $\lambda / n$

| Frequency (GHz) | *n* | *N* | *cond* |
|---|---|---|---|
| 0.1 | 10 | 257 | $1.4*10^5$ |
| | 20 | 513 | $2.2*10^6$ |
| | 40 | 897 | $3.1*10^5$ |
| 0.5 | 10 | 1153 | $2.7*10^5$ |
| | 20 | 2177 | $5.7*10^5$ |
| | 40 | 4353 | $9.6*10^6$ |
| 1 | 10 | 2177 | $8.2*10^4$ |
| | 20 | 4353 | $1.6*10^5$ |
| | 40 | 8705 | $6.4*10^5$ |

Preprints (www.preprints.org) | NOT PEER-REVIEWED | Posted: 6 June 2022 doi:10.20944/preprints202206.0061.v1



**Table 2**. The input impedance values for the biconical AE with $a$ = 508 mm and $\Theta_1 = \Theta_2 = 53.1°$ at frequencies of 0.1, 0.2, and 1 GHz and a mesh step (segment size) $\lambda / n$

| Frequency (GHz) | $n$ | (A1), (A11) | EMPro | Wire-grid |
|---|---|---|---|---|
| 0.1 | 10 | 40.40 + j28.32 | 29.73 + j15.78 | 0.46 – j25.48 |
| | 20 | | 39.51 + j12.95 | 192.31 – j58.89 |
| | 40 | | – | 28.01 + j25.59 |
| 0.5 | 10 | 101.80 – j9.38 | 117.48 + j64.27 | 114.01 – j6.29 |
| | 20 | | 112.89 + j74.69 | 102.02 + j33.36 |
| | 40 | | – | 90.44 + j48.18 |
| 1 | 10 | 88.64 + j16.68 | 116.40 + j89.92 | 103.11 + j41.34 |
| | 20 | | 117.84 + j112.36 | 88.29 + j56.82 |
| | 40 | | – | 84.62 + j71.55 |

**Table 3**. The deviation (%) of the input impedance magnitudes from Table 2 calculated using the wire-grid and EMPro comparing to those obtained analytically

| Frequency (GHz) | $n$ | EMPro | Wire-grid |
|---|---|---|---|
| 0.1 | 10 | 31.78 | 48.35 |
| | 20 | 15.73 | 307.65 |
| | 40 | – | 23.10 |
| 0.5 | 10 | 30.99 | 11.69 |
| | 20 | 32.41 | 4.99 |
| | 40 | – | 0.23 |
| 1 | 10 | 63.08 | 23.16 |
| | 20 | 80.52 | 16.41 |
| | 40 | – | 22.86 |

**Table 4**. The elapsed time and used memory for simulating the biconical AE using the wire-grid, with $a$ = 508 mm and $\Theta_1 = \Theta_2 = 53.1°$
at frequencies of 0.1, 0.2, and 1 GHz and a mesh step (segment size) $\lambda / n$

| Frequency (GHz) | $n$ | $T$ (s) | $M$ (MB) |
|---|---|---|---|
| 0.1 | 10 | 0.34 | 1 |
| | 20 | 0.51 | 4 |
| | 40 | 0.60 | 12.28 |
| 0.5 | 10 | 1.02 | 20.29 |
| | 20 | 4.11 | 72.31 |
| | 40 | 19.29 | 289.13 |
| 1 | 10 | 4.03 | 72.31 |
| | 20 | 18.29 | 289.13 |
| | 40 | 109.06 | 1156.27 |

Preprints (www.preprints.org) | NOT PEER-REVIEWED | Posted: 6 June 2022 doi:10.20944/preprints202206.0061.v1



**Table 5**. The elapsed time to obtain the RTC at each frequency, the total simulation time ($T_t$) and the used memory for simulating the biconical AE using EMPro, with $a$ = 508 mm and $\Theta_1 = \Theta_2 = 53.1°$at frequencies of 0.1, 0.2, and 1 GHz and a mesh step (segment size) $\lambda / n$.

| $n$ | Frequency (GHz) | $T$ (s) | $T_t$ (s) | Physical/virtual memory (MB) | Required (GB) | Problem size (cells) |
|---|---|---|---|---|---|---|
| 10 | 0.1 | 159 | 921 | 903/922 | 1.2 | 331*311*245 |
| | 0.5 | 181 | | | | |
| | 1 | 183 | | | | |
| 20 | 0.1 | 567 | 1892 | 4722/4753 | 6 | 584*581*448 |
| | 0.5 | 649 | | | | |
| | 1 | 676 | | | | |
| 40 | 0.1 | – | – | – | 36 | 1126*1120*855 |
| | 0.5 | – | | – | | |
| | 1 | – | | – | | |

Figures 10–12 show the RP obtained using the wire-grid with decreasing mesh size (segments number) at frequencies of 0.1, 0.2 and 1 GHz, respectively. Additionally, for clarity, similar results obtained in EMPro are given.

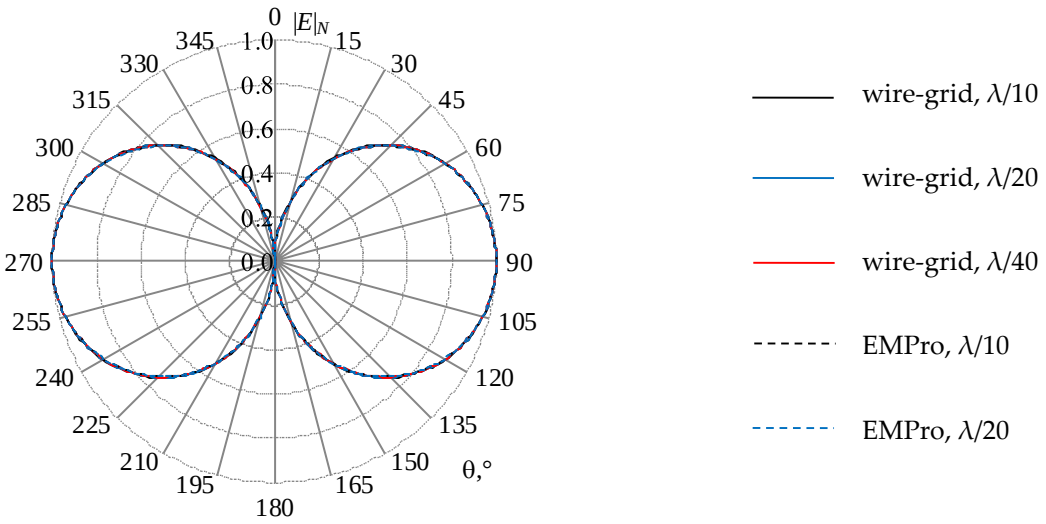


Figure 10. The normalized RP ($|E|_N$, times) of the biconical AE with $a$ = 508 mm and $\Theta_1 = \Theta_2 = 53.1°$ when $ka_1 = 1.0640$ ($f_1$ = 0.1 GHz), calculated by the wire-grid and EMPro

Preprints (www.preprints.org) | NOT PEER-REVIEWED | Posted: 6 June 2022 doi:10.20944/preprints202206.0061.v1



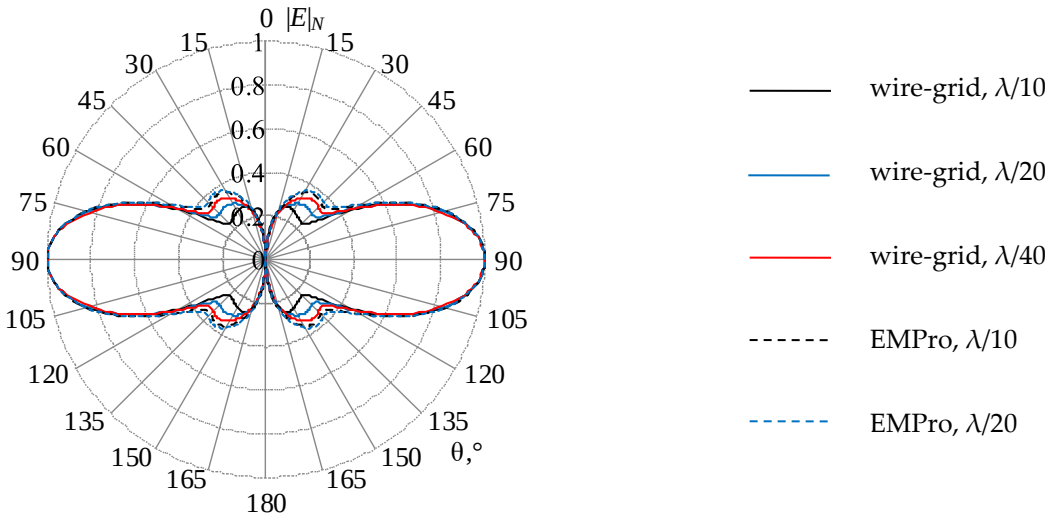


Figure 11. The normalized RP ($|E|_N$, times) of the biconical AE with $a$ = 508 mm and $\Theta_1 = \Theta_2 = 53.1°$ when $ka_2$ = 5.3198 ($f_1$ = 0.5 GHz), calculated by the wire-grid and EMPro

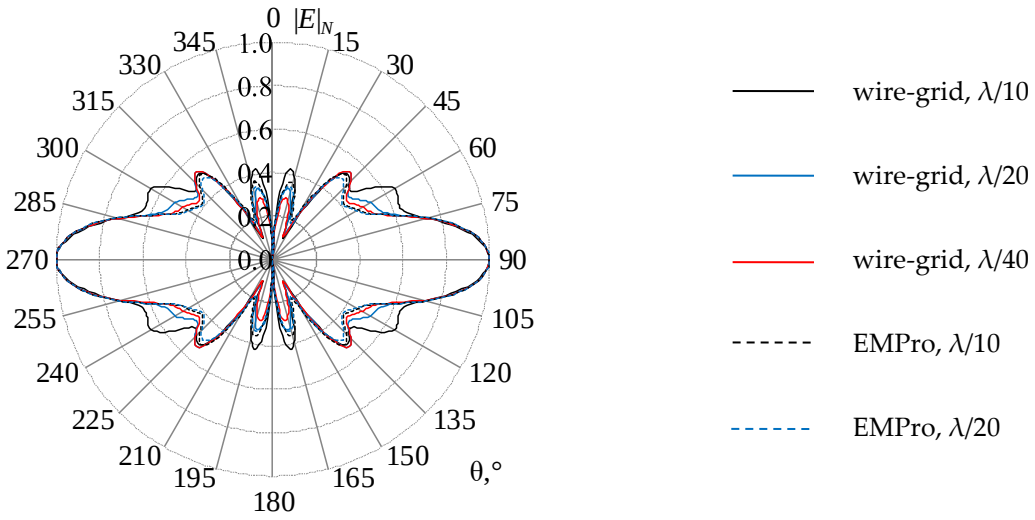


Figure 12. The normalized RP ($|E|_N$, times) of the biconical AE with $a$ = 508 mm and $\Theta_1 = \Theta_2 = 53.1°$ when $ka_3$ = 10.6395 ($f_1$ = 1 GHz), calculated by the wire-grid and EMPro

In figures 16–18 the results obtained by using the wire-grid, the EMPro (FDTD) system ($\lambda$/10 mesh was used in the further comparisons since it's results seem to be closer to the analytical ones), and the analytical expressions are summarized. In general, all the results are consistent with each other. Table 6 shows the largest differences in the calculated values compared to those obtained by(A8).

Preprints (www.preprints.org) | NOT PEER-REVIEWED | Posted: 6 June 2022 doi:10.20944/preprints202206.0061.v1



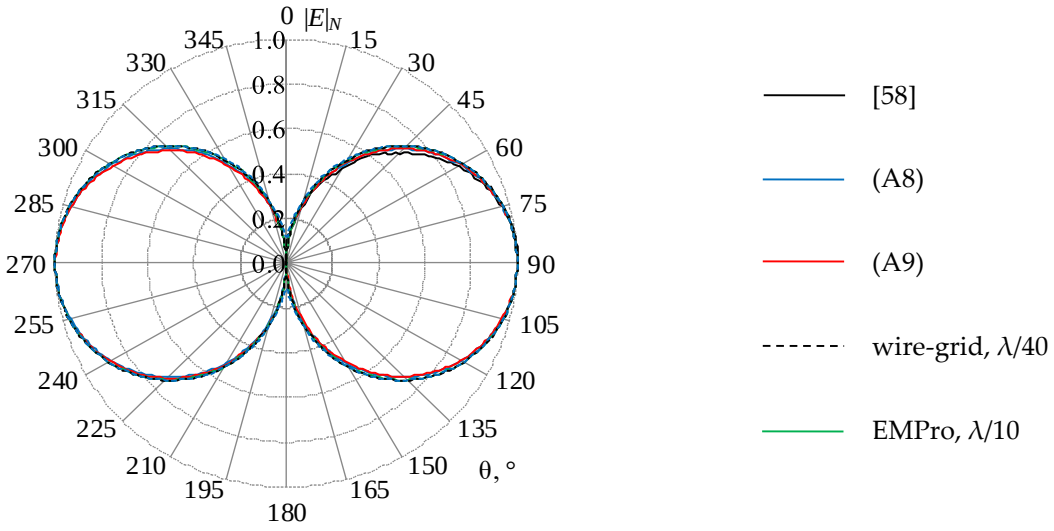


Figure 13. The normalized RP ($|E|_N$, times) of the biconical AE when $ka_1 = 1.0640$ ($f_1 = 0.1$ GHz), calculated analytically and by the wire-grid and EMPro at different mesh sizes

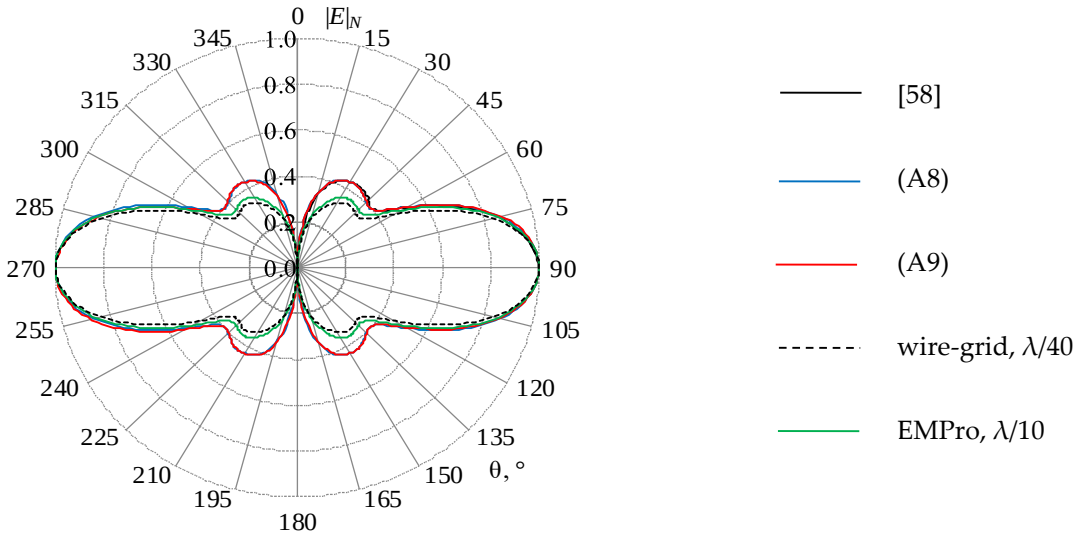


Figure 14. The normalized RP ($|E|_N$, times) of the biconical AE when $ka_2 = 5.3198$ ($f_1 = 0.5$ GHz), calculated analytically and by the wire-grid and EMPro at different mesh sizes

Preprints (www.preprints.org) | NOT PEER-REVIEWED | Posted: 6 June 2022 doi:10.20944/preprints202206.0061.v1



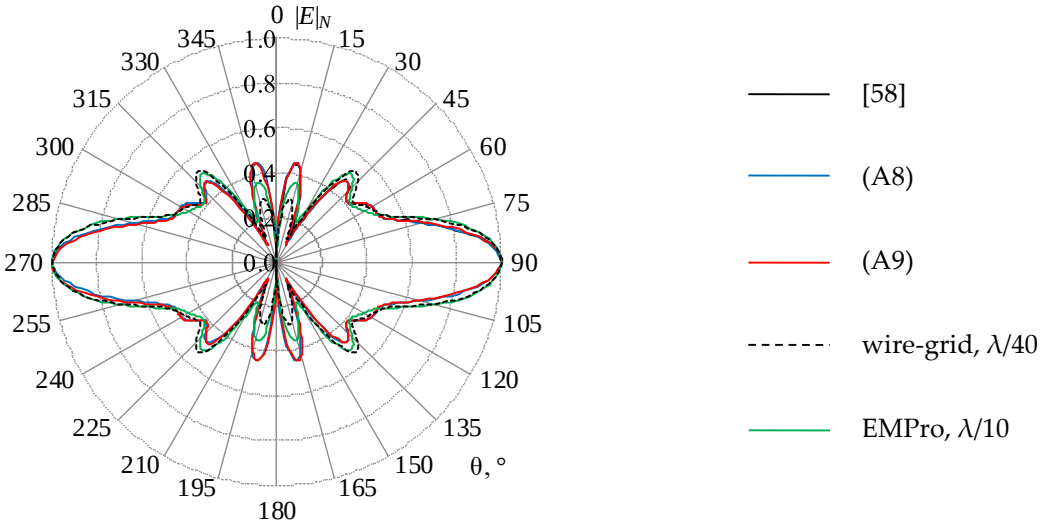


Figure 15. The normalized RP ($|E|_N$, times) of the biconical AE when $ka_3 = 10.6395$ ($f_1 = 1$ GHz), calculated analytically and by the wire-grid and EMPro at different mesh sizes

**Table 6**. The maximum differences of normalized RP values obtained at different mesh sizes $\lambda / n$ and by (A8) at frequencies of 0.1, 0.2, and 1 GHz

| Frequency (GHz) | *n* | EMPro | Wire-grid |
|---|---|---|---|
| 0.1 | 10 | 0.0189 | 0.0259 |
| | 20 | 0.0189 | 0.0236 |
| | 40 | – | 0.0211 |
| 0.5 | 10 | 0.1080 | 0.1869 |
| | 20 | 0.1030 | 0.1395 |
| | 40 | – | 0.1395 |
| 1 | 10 | 0.1291 | 0.1569 |
| | 20 | 0.1268 | 0.1197 |
| | 40 | – | 0.1669 |

As can be seen from Table 2–6 and Figures 10–18, the estimated RTC AE results and their calculation error using the wire-grid were compared to those obtained analytically and using the EMPro system. It is shown how the decrease in the grid step affects the obtained values of the RP and the input impedance. The RPs obtained using the wire-grid are close to those obtained using the analytical expressions. At the same time, the computational costs when using the wire-grid are much less than those obtained using the EMPro system. The obtained results proved that using the proposed recommendations for modeling the symmetrical biconical AE can give accurate results and with less computational costs.

### *3.3. Modeling horn AE*

Another complex structure to be modeled is a horn AE presented in (Figure 16). The cross section of this AE is symmetrical in two planes. This AE is also simulated and tested using the wire-grid approximation, and new recommendations for modeling it are determined and provided further. The inner surface geometrical parameters of this AE are presented in Table 7. The wall thickness of the regular part of the AE is 1 mm, and the irregular part is 2 mm. For verifying the obtained results of modeling the horn RTCs, the results are compared with the measured ones for a manufactured prototype of this horn (its parameters after manufacturing are measured and also presented in Table 7). The AE was

Preprints (www.preprints.org) | NOT PEER-REVIEWED | Posted: 6 June 2022 doi:10.20944/preprints202206.0061.v1



modeled using the wire-grid at an operating frequency of 8 GHz. The AE was excited by installing a wire at the junction of the regular and irregular parts of the horn between its wide walls. The length of the wire corresponded to the value $b$ from Table 7. The wire was approximated by one segment. After performing model-testing based on the wire-grid approximation model, the following recommendations were obtained for modeling these types of AEs.

For common issues, a wide range of parameters was used. The RTCs of the AE were calculated with a decrease in the mesh step of the grid $\lambda / n$ and an increase in the number of wires to approximate the surface of the regular part of the AE. When modeling, the wide walls of the regular part (the index $r$ is used to denote the regular part of the AE) were divided into $SZ_r$ parts along the $z$ axis and $SX_r$ parts along the $x$ axis, the narrow sides were $SZ_r$ and $SY_r$, and the back shortened wall was divided into $SX_r$ and $SY_r$, respectively. The ratios $SZ_r = SX_r = L_r$, $SY_r = L_r / 2$ were used. To approximate the extended part of horn (the index $e$ is used to denote the extended part of the AE) its wide walls were divided into $SZ_e$ parts on the $z$ axis and $SX_e$ parts along the $x$ axis, and narrow ones – $SY_e$ parts along the $y$ axis. It is assumed that $SY_e = SX_e / 2$ and the ratios $SZ_e = SX_e = L_e$, $SY_e = L_e / 2$ were used. The order $N$ of the SLAE matrix $\mathbf{Z}$ with using the values of $n = 10, 20, 40$, $L_e = 16$ for the irregular part of the horn AE, and $L_r = 2, 4, 8, 16$ for the regular part, are given in Table 8. Moreover, the condition numbers for matrix $\mathbf{Z}$ are presented along with the time consumed to calculate them, as well as the total numbers of wire used to model the regular and the extended parts of the AE. General views of the AE with the $L_r$ values are shown in Figure 17. The values $L_e = 16$ and $L_r = 8$ seem to be minimal optimal values (see Appendix B) for modeling such AEs. The calculated values of the normalized magnitude of the electric field strength ($|E|_N$, dB) at $\varphi = 0°$ и $\varphi = 90°$ are shown in Figure 18, and demonstrate convergence with an increase of $n$. Therefore, the value $n = 40$ seems to be optimal. The values of the segment length $l_s$, the radius of the structure wires $a_s$ and the radius of the wire where the excitation was applied $a_{ex}$, were determined as $l_s = \lambda / n$, $a_s = l_s / 10$, $a_{ex} = l_s / 5$, respectively. The wire where the excitation was applied was approximated by one segment.

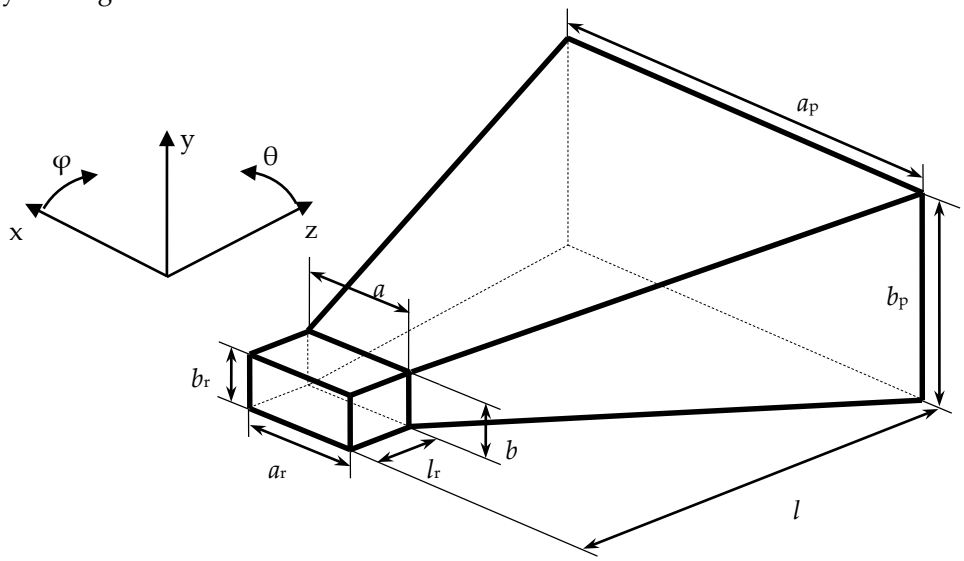


Figure 16. The isometric view of the inner surface of the horn AE

**Table 7**. The geometrical parameters (mm) of the inner surface of the horn AE

| Geometrical parameter | $a_p$ | $b_p$ | $a$ | $b$ | $a_r$ | $b_r$ | $l$ | $l_r$ |
|---|---|---|---|---|---|---|---|---|
| Model | 80 | 60 | 23 | 10 | 23 | 10 | 150 | 10 |
| Prototype | 79.9 | 59.8 | 23.0 | 10.0 | 23.0 | 10.0 | 149.9 | 10.0 |

Preprints (www.preprints.org) | NOT PEER-REVIEWED | Posted: 6 June 2022 doi:10.20944/preprints202206.0061.v1



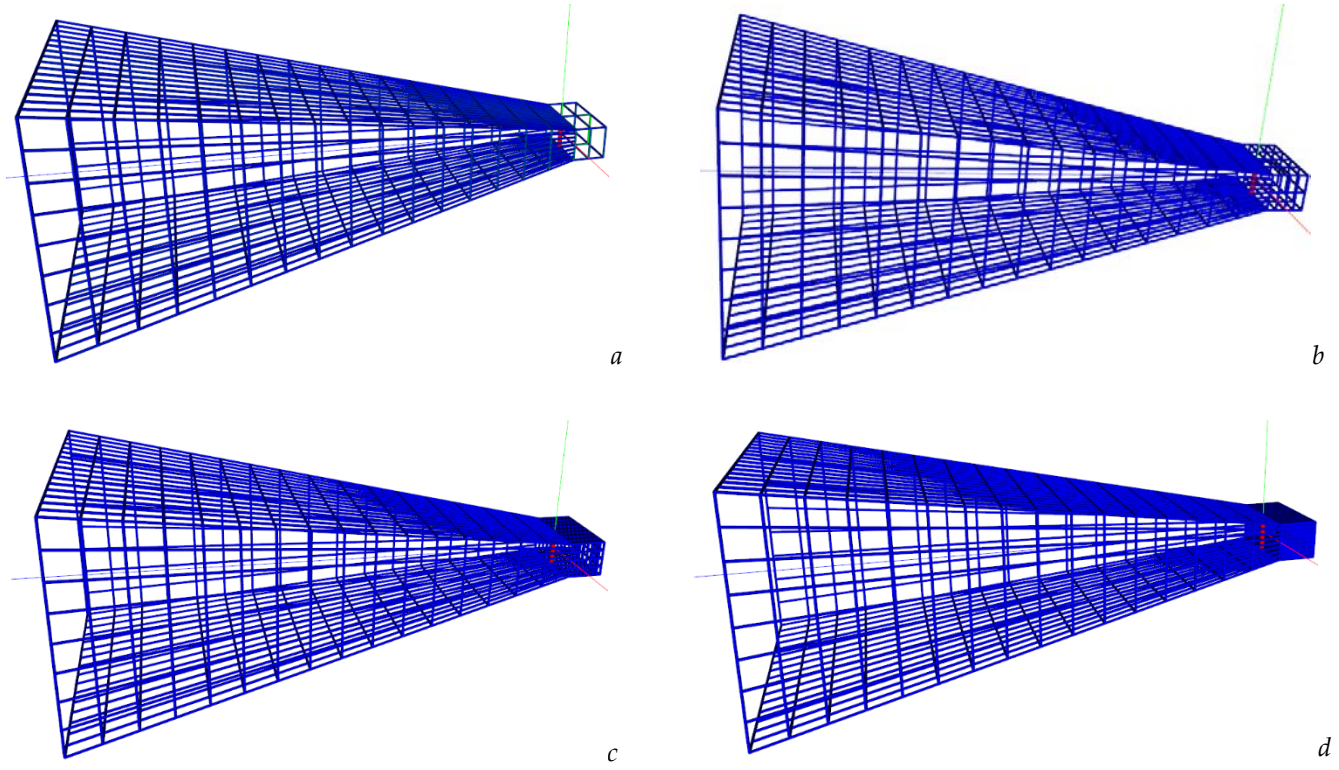


Figure 17. General views of AEs with the wire used as an excitation source built in the wire-grid using $L_e = 16$ and $L_r = 2$ (*a*), 4 (*b*), 8 (*c*), and 16 (*d*)

**Table 8**. Total wire number (*TWN*) and the order *N* of the SLAE matrix **Z** for the horn AE at different mesh step of the grid $\lambda / n$ using the wire-grid and $L_e = 16$, and $L_r = 2, 4, 8, 16$; the condition number for matrix **Z** (*cond*) and the time consumed to calculate **Z** (*T*).

| | | ***n*** | | | | | | | | |
|---|---|---|---|---|---|---|---|---|---|---|
| $L_r$ | *TWN* | **10** | | | **20** | | | **40** | | |
| | | ***N*** | ***T* (s)** | ***cond*** | ***N*** | ***T* (s)** | ***cond*** | ***N*** | ***T* (s)** | ***cond*** |
| 2 | 1609 | 3544 | 1.65 | $2.35*10^4$ | 5931 | 4.40 | $8.68*10^4$ | 11448 | 16.80 | $3.76*10^5$ |
| 4 | 1687 | 3636 | 1.71 | $2.41*10^4$ | 6112 | 4.73 | $8.91*10^4$ | 11742 | 17.46 | $1.89*10^6$ |
| 8 | 1999 | 3906 | 2.01 | $3.28*10^4$ | 6480 | 5.25 | $1.02*10^5$ | 12464 | 19.25 | $4.48*10^5$ |
| 16 | 3247 | 5178 | 3.44 | $3.69*10^5$ | 7556 | 7.10 | $2.07*10^6$ | 13936 | 24.49 | $9.81*10^5$ |

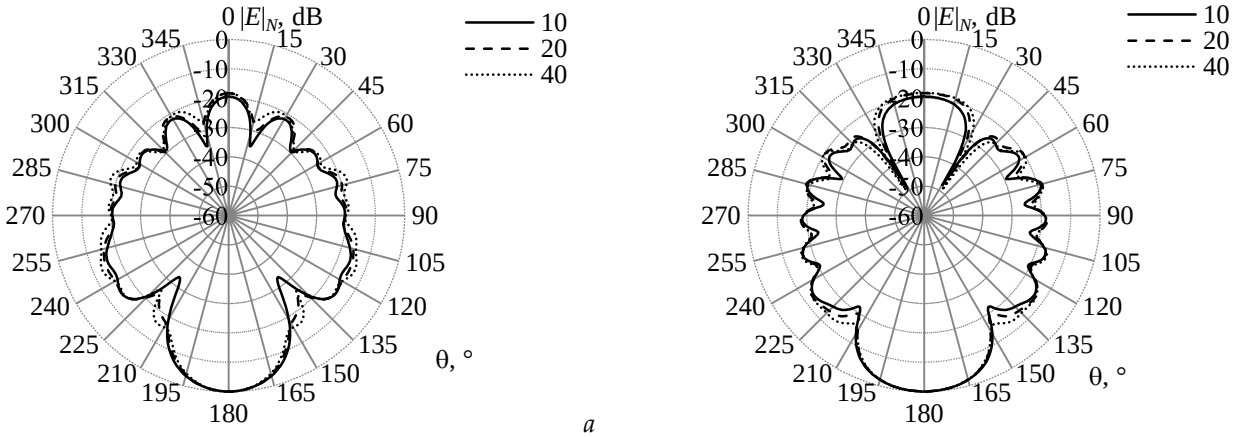


Figure 18. The RPs ($|E|_N$, dB) of the horn AE at the frequency of 8 GHz in the $\varphi = 90°$ (*a*) and $\varphi = 0°$ (*b*) planes in the wire-grid with $L_e = 16$ and $L_r = 8$, $n = 10, 20, 40$

Preprints (www.preprints.org) | NOT PEER-REVIEWED | Posted: 6 June 2022 doi:10.20944/preprints202206.0061.v1



The prototype of the horn AE with the parameters presented in Table 7 was manufactured, and its RTCs were measured in order to validate the results calculated using the wire-grid approximation. Figure 19 compares the results of the normalized RPs obtained using the wire-grid ($L_r$ = 8, $SX_e$ = $SZ_e$ = 16) and experimentally at φ = 0° and φ = 90°. Table 9 summarizes the calculated and the measured AE main beamwidths (*BW*) and the levels of the sidelobes ($SL_{max}$).

**Table 9**. The calculated and measured RTCs of the horn AE

| RTC | Wire-grid | Measured |
|---|---|---|
| *BW* (°), φ = 90° | 25 | 31 |
| *BW* (°), φ = 0° | 34 | 31 |
| $SL_{max}$ (dB) | –12.61 | -16.93 |

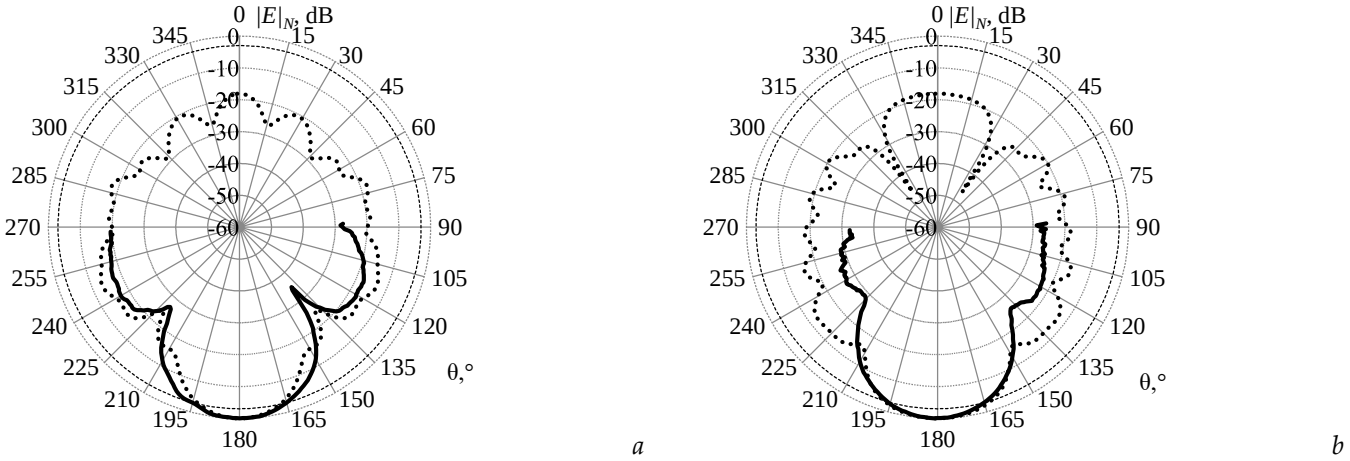


Figure 19. The measured (—) and the calculated (····) RPs ($|E|_N$, dB) of the horn AE at the frequency of 8 GHz in the φ = 90° (*a*) and φ = 0° (*b*) planes in the wire-grid with $L_e$ = 16 and $L_r$ = 8, *n* = 40. The level of –3 dB (---).

Then we compared the results of simulation with the changing of the grid to the measured results. Figures 20–22 show the RPs for the horn AE using $L_r$ = 8, 16, 32 and $L_e$ = 16, 32 and $SZ_e$ = $SX_e$ or equal to $SX_e$*$2^{\pm1}$. Figure 23 summarizes these results together for clarity and the numbers in the graphics legend refer to $L_r$, $SX_e$, $SZ_e$, respectively. As can be seen from Figures 20–23, if the grid cells are refined to have a closer to square shape, the obtained results can be closer to the measured ones. Note that the results using the same value for $SZ_e$ are very close except at the back lobe where the denser grid gives less radiation level. Therefore, one can say that the optimal grid form is symmetrical, denser, and squarer. This corresponds to $SZ_e$ = $SX_e$=32. Figure 24 compares the results considering this point. It can be seen that the results are almost identical and increasing the density of the grid will not produce more accurate results, but will only increase the computational costs as can be seen from Table 10 in which the calculated condition numbers and the input impedance (*Z*=*R*+j*X*) of the horn AE and the time consumed to calculate them at different mesh and grid settings using wire-grid approximation are presented.

Preprints (www.preprints.org) | NOT PEER-REVIEWED | Posted: 6 June 2022 doi:10.20944/preprints202206.0061.v1



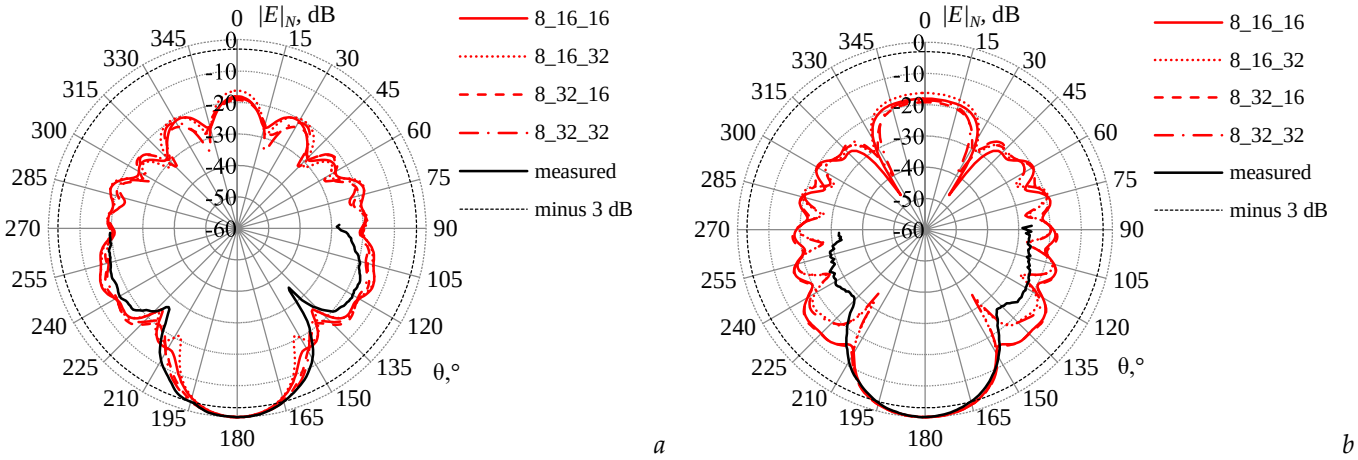


Figure 20. The measured and the calculated RPs ($|E|_N$, dB) of the horn AE at the frequency of 8 GHz in the φ = 90° (*a*) and φ = 0° (*b*) planes in the wire-grid with $L_r$ = 8, $n$ = 40, $L_e$ = 16, 32 and $SZ_e = SX_e$ or equal to $SX_e*2^{\pm1}$. The level of –3 dB (---).

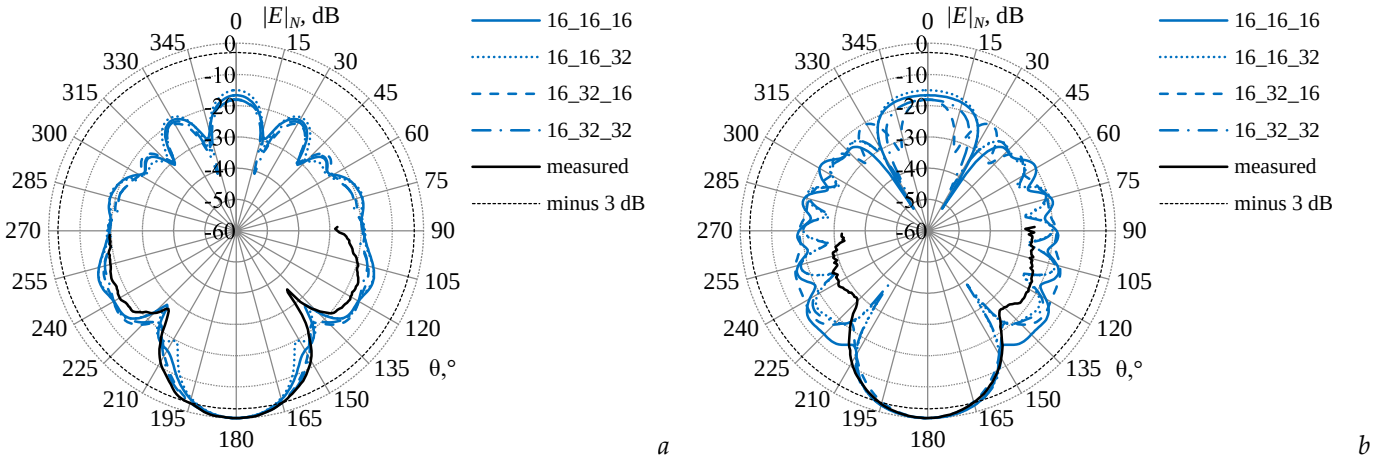


Figure 21. The measured and the calculated RPs ($|E|_N$, dB) of the horn AE at the frequency of 8 GHz in the φ = 90° (*a*) and φ = 0° (*b*) planes in the wire-grid with $L_r$ = 16, $n$ = 40, $L_e$ = 16, 32 and $SZ_e = SX_e$ or equal to $SX_e*2^{\pm1}$. The level of –3 dB (---).

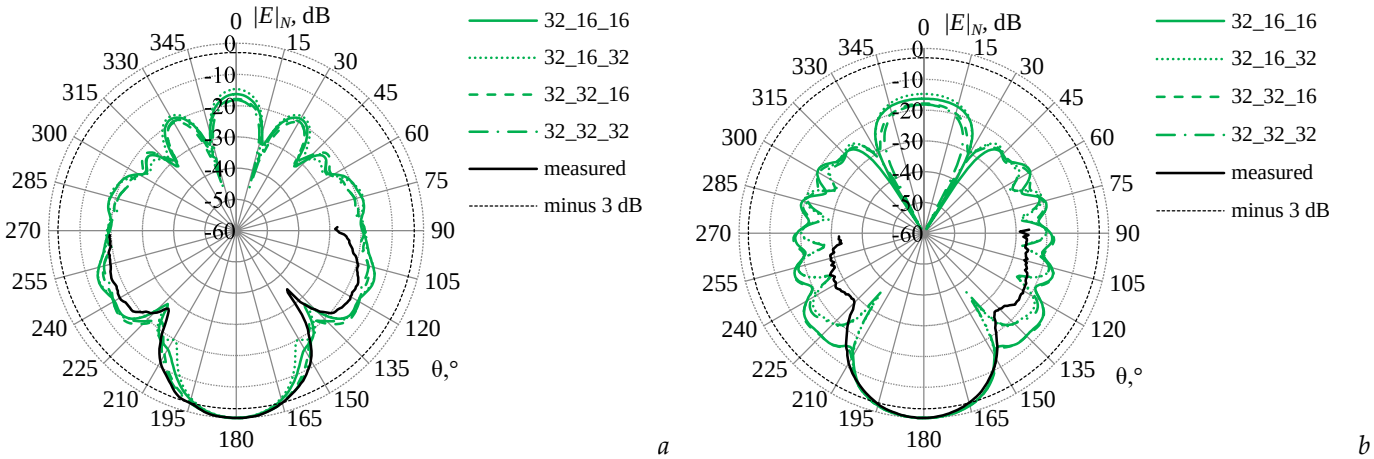


Figure 22. The measured and the calculated RPs ($|E|_N$, dB) of the horn AE at the frequency of 8 GHz in the φ = 90° (*a*) and φ = 0° (*b*) planes in the wire-grid with $L_r$ = 32, $n$ = 40, $L_e$ = 16, 32 and $SZ_e = SX_e$ or equal to $SX_e*2^{\pm1}$. The level of –3 dB (---).

Preprints (www.preprints.org) | NOT PEER-REVIEWED | Posted: 6 June 2022 doi:10.20944/preprints202206.0061.v1



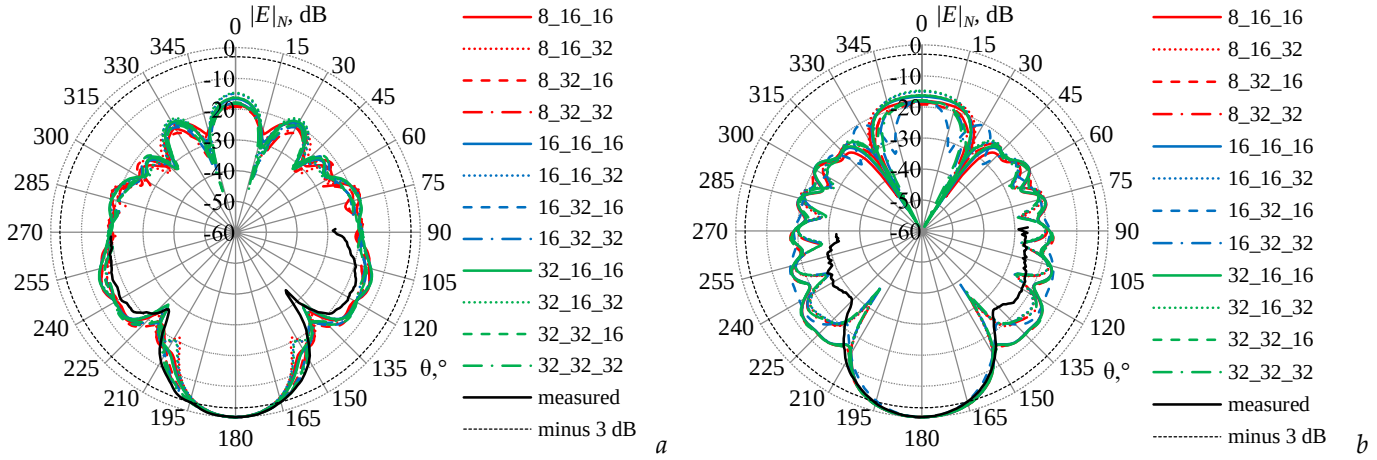


Figure 23. The measured and the calculated RPs ($|E|_N$, dB) of the horn AE at the frequency of 8 GHz in the φ = 90° (*a*) and φ = 0° (*b*) planes in the wire-grid with $L_r$ = 8, 16, 32, $n$ = 40, $L_e$ = 16, 32 and $SZ_e = SX_e$ or equal to $SX_e*2^{\pm1}$. The level of –3 dB (---).

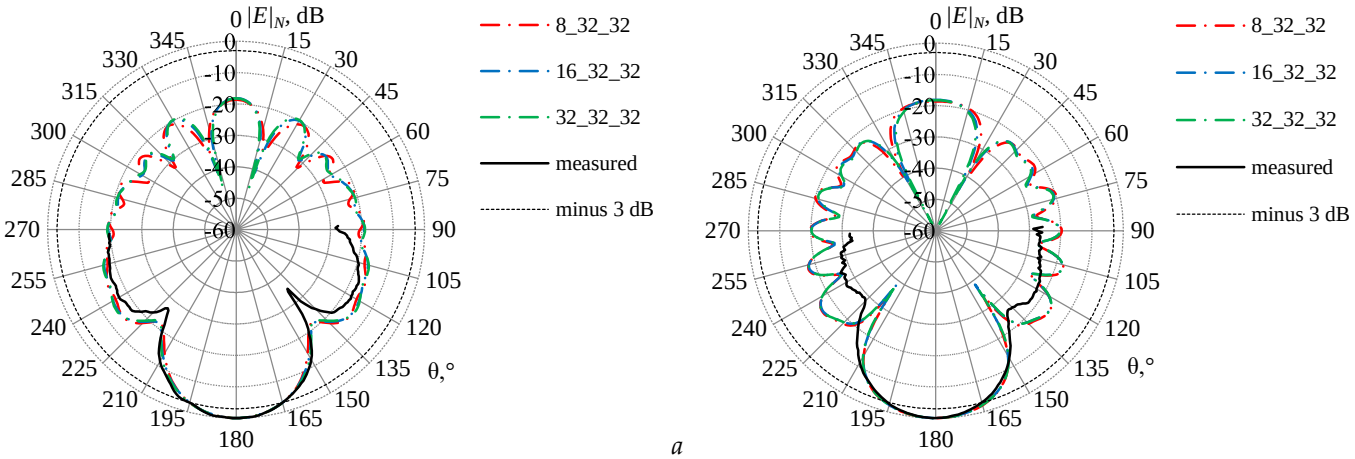


Figure 24. The measured and the calculated RPs ($|E|_N$, dB) of the horn AE at the frequency of 8 GHz in the φ = 90° (*a*) and φ = 0° (*b*) planes in the wire-grid with $L_r$ = 8, 16, 32, $n$ = 40, $L_e$ = 32 and $SZ_e = SX_e$. The level of –3 dB (---).

Preprints (www.preprints.org) | NOT PEER-REVIEWED | Posted: 6 June 2022 doi:10.20944/preprints202206.0061.v1



**Table 10**. The calculated RTCs of the horn AE using the wire-grid with different mesh and grid settings

| | | | | | | | | | | | | | | | | | | | | |
|---|---|---|---|---|---|---|---|---|---|---|---|---|---|---|---|---|---|---|---|---|
| | | | | | | | | | | | | | *n* | | | | | | | |
| | | | | | 10 | | | | | | 20 | | | | | | 40 | | | |
| $L_r$ | 8 | | 16 | | 32 | | 8 | | 16 | | 32 | | 8 | | 16 | | 32 | | | |
| $SX_e$ | 16 | 32 | 16 | 32 | 16 | 32 | 16 | 32 | 16 | 32 | 16 | 32 | 16 | 32 | 16 | 32 | 16 | 32 | 16 | 32 |
| $SZ_e$ | 16 | 32 | 16 | 32 | 16 | 32 | 16 | 32 | 16 | 32 | 16 | 32 | 16 | 32 | 16 | 32 | 16 | 32 | 16 | 32 |
| *TWN* | 1584+415 | 3120+415 | 3168+415 | 6240+415 | 1584+1663 | 3120+1663 | 3168+1663 | 6240+1663 | 1584+6655 | 3120+6655 | 3168+6655 | 6240+6655 | 1584+415 | 3120+415 | 3168+415 | 6240+415 | 1584+1663 | 3120+1663 | 3168+1663 | 6240+1663 |
| *N* | 3906 | 5794 | 6674 | 9746 | 5178 | 7066 | 7946 | 11018 | 10218 | 12106 | 12986 | 16058 | 6480 | 9120 | 10688 | 14464 | 7556 | 10196 | 11764 | 15540 |
| *T* (s) | 6.42 | 15.12 | 21.60 | 52.72 | 12.43 | 24.05 | 31.47 | 64.34 | 54.28 | 83.22 | 97.87 | 167.24 | 19.10 | 41.30 | 61.06 | 131.29 | 27.56 | 55.39 | 77.57 | 157.34 |
| *cond* | $3.28*10^4$ | $5.02*10^4$ | $7.37*10^4$ | $1.50*10^5$ | $3.69*10^5$ | $4.50*10^5$ | $4.72*10^5$ | $6.05*10^5$ | $2.75*10^7$ | $3.12*10^7$ | $5.10*10^7$ | $5.91*10^7$ | $1.03*10^5$ | $1.26*10^5$ | $1.80*10^5$ | $2.60*10^5$ | $2.07*10^6$ | $2.49*10^6$ | $2.56*10^6$ | $3.15*10^6$ |
| *R* (Ohm) | 227.18 | 298.17 | 231.90 | 303.70 | 217.05 | 287.70 | 224.36 | 290.93 | 217.33 | 287.74 | 222.93 | 289.09 | 215.68 | 274.68 | 226.40 | 293.19 | 205.07 | 264.48 | 216.17 | 279.08 |
| *X* (Ohm) | 267.54 | 274.63 | 267.14 | 288.83 | 275.49 | 290.37 | 275.55 | 304.27 | 277.11 | 292.70 | 276.17 | 305.65 | 330.36 | 306.99 | 326.06 | 321.58 | 341.40 | 328.61 | 339.68 | 346.79 |
| \|Z\| (Ohm) | 349.05 | 405.37 | 353.76 | 419.12 | 350.73 | 408.76 | 355.34 | 420.98 | 352.16 | 410.44 | 354.92 | 167.24 | 394.50 | 411.94 | 396.95 | 435.17 | 398.26 | 421.83 | 402.63 | 445.14 |
| | $5.28*10^6$ | $5.80*10^6$ | $5.96*10^6$ | $6.77*10^6$ | $4.48*10^5$ | $4.58*10^5$ | $8.76*10^5$ | $7.89*10^5$ | $9.81*10^5$ | $1.07*10^6$ | $1.40*10^6$ | $1.44*10^6$ | $2.94*10^6$ | $3.15*10^6$ | $3.50*10^6$ | $3.72*10^6$ | | | | |
| | 204.48 | 263.96 | 2113.53 | 275.19 | 210.86 | 242.17 | 221.74 | 275.12 | 199.63 | 234.12 | 212.97 | 266.42 | 193.60 | 228.65 | 207.58 | 259.63 | | | | |
| | 345.87 | 335.80 | 342.88 | 352.96 | 400.66 | 366.40 | 389.78 | 368.76 | 415.03 | 388.28 | 407.21 | 399.02 | 419.44 | 395.82 | 413.16 | 409.90 | | | | |
| | 401.79 | 427.13 | 403.93 | 447.57 | 452.75 | 439.20 | 448.43 | 460.08 | 460.55 | 453.40 | 459.54 | 479.79 | 461.96 | 457.11 | 462.38 | 485.20 | | | | |

## 4. Conclusions

In this paper we focused on the use of the MoM and wire-grid approximation as an effective computational approach for modeling symmetrical AEs with low computational cost and quite accurate results. For AE modeling, the MoM using RWG basic functions is widely used nowadays. The use of this method leads to reducing the integral equation to SLAE, the order of which determines the required machine memory. Therefore, it is advisable to search for other ways to save machine computational resources while maintaining the required modeling accuracy.

One such approach is the wire-grid, which replaces the conductive surfaces of the AE with a grid of wires. This will not only reduce the computational costs, but it may also give an equivalent structure of the AE with less mass if it's available to manufacture in its new form. However, this approach is complicated because it is necessary to construct the grid of wires correctly. To do this, there are several recommendations that are nonuniversal (they do not allow modeling arbitrary constructions) and difficult in software implementation.

Recommendations from various sources including criteria and conditions for the use of wire-grid surface approximation for AE modeling are summarized in this work. New recommendations are proposed for modeling symmetrical biconical and horn AE structures. The proposed recommendations are used to calculate the characteristics of biconical AE at different frequencies. The calculated results are compared to the ones obtained analytically using well-known Legendre and Hankel functions. These results showed a good agreement not only with analytical results but also with those obtained using another numerical method such as the FDTD method.

By the same token, we verified the proposed wire-grid approximation modeling recommendations on the commonly used horn AE. The received radiation patterns are compared to the measured ones and to the results obtained using the FDTD. The results are compared and analyzed using different grid and mesh settings. It was revealed that the closer symmetrical grid cells form to square shape, the more accurate results can be obtained with low computational cost. Additionally, we show the modification of the known equal area rule on a rectangular grid form. The obtained radiation patterns of a conductive plate using the original rule and the modified one are compared with the FDTD electrodynamic analysis results. It is shown that the use of the modified rule is more suitable in this case.

In general, this approach along with the proposed recommendations showed its ability to give accurate results comparing to the obtained analytically, numerically and experimentally. Moreover, it surpasses other methods in the required computational time and memory to get the same results.

However, the recommendations cannot be applied on arbitrary structures. They have been tested only on such AE as the ones used in this work. In the case of a radical or complex changes in the structure, it is imperative to adjust them to meet all the special requirements which every unique structure demands and eliminate any other unnecessary elements or dependences. For example, when modeling the biconical AE, we didn't use the horizontal grid elements because the current distributed among them is slightly affects the desired RTCs. On the contrary, in the case of the horn AE, the use of them was unavoidable since they have a remarkable impact on the horn AE RP back lobe. It is also worthwhile to consider the relationship between some elements and the wavelengths when building the grid of wires, which can lead to a number of restrictions on using the wire-grid approximation as for instance, the segment length/radius ratio or the distance between the wires. This will deliver a number of limitations on the use of the wire-grid to deal with, added to those of the MoM.

Furthermore, building the grid by itself and testing it considering all these possibilities and limitations is a challenge and a time-consuming issue. Consequently, beside the fact that using this approach seems to be promising, it is relevant to make it easier and more efficient. One of the perspective developments of the module used in this study is to add new capabilities which can enable it to import any AE geometrical model from a third-part computer aided design system and independently build and refine its equivalent wire-grid considering all the possible limitations and using the proposed modeling recommendations. Another future improvement is to create a smooth user interface for this module to enhance the user experience. Likewise, expansion the module database of different AE structures and universalizing the recommendations proposed here can carry off a core for an advanced and expert AEs modeling software system.

 doi:10.20944/preprints202206.0061.v1



**Author Contributions:** Conceptualization, A.A.H. and S.P.K.; methodology, S.P.K. and A.A.H.; software, A.A.K. and A.A.H; validation, M.E.K., A.A.H. and D.V.K.; formal analysis, A.A.H. and S.P.K.; investigation, A.A.H; resources, S.P.K.; data curation, D.V.K.; writing—original draft preparation, S.P.K.; writing—review and editing, A.A.H; visualization, A.A.H and A.A.K; supervision, S.P.K.; project administration, A.A.H. All authors have read and agreed to the published version of the manuscript.

**Funding:** This research was funded by the Ministry of Science and Higher Education of the Russian Federation project FEWM-2022-0001.

**Conflicts of Interest:** The authors declare no conflict of interest.

Preprints (www.preprints.org) | NOT PEER-REVIEWED | Posted: 6 June 2022 doi:10.20944/preprints202206.0061.v1



## Appendix A

Here, the analytical expressions from [57–59] used to obtain the digitized data of the conical and biconical AE are presented. The input impedance $Z_{in}$ of a conical AE Figure 8 *a* powered by a coaxial transmission line is defined as [57]

$$Z_{in} = Z_0 \frac{1-\beta/\alpha}{1+\beta/\alpha} \tag{A1}$$

where $Z_0$ is the characteristic impedance of the AE with a given opening angle of the cone $\Theta_0$, defined as

$$Z_0 = 60 \ln\left(\mathrm{ctg}(\Theta_0/2)\right) \tag{A2}$$

and the ratio of the amplitudes of reflected (β) and outwardly propagating (α) TEM-waves outside in the antenna region as

$$\beta/\alpha = e^{-2ika} \frac{1+i\frac{60}{Z_0}\sum_{n=1}^{\infty}\frac{2n+1}{n(n+1)}\left[P_n(\cos(\Theta_0))\right]^2 \zeta(ka)}{-1+i\frac{60}{Z_0}\sum_{n=1}^{\infty}\frac{2n+1}{n(n+1)}\left[P_n(\cos(\Theta_0))\right]^2 \zeta(ka)} \tag{A3}$$

where $P_n(\cos(\Theta_0))$ is a Legendre polynomial of order $n$, $\zeta(ka)$ is an auxiliary function of real variable $ka$ (where $k = 2\pi/\lambda$, $a$ – a cone size from Figure 8), which is defined through the spherical Hankel functions of the 2nd type and the nth order as

$$\zeta(ka) = \frac{h_n^{(2)}(ka)}{h_{n-1}^{(2)}(ka) - \frac{n}{ka} h_n^{(2)}(ka)}. \tag{A4}$$

The cylindrical Hankel functions of the 1st and 2nd type of order $n$ can be found with respect to the Bessel functions $j_n(x)$ and $y_n(x)$ of the 1st and 2nd type, respectively, for $n \in J$, $x \in [0, \infty]$

$$h_n^{(1)} = j_n(x) + iy_n(x), \tag{A5}$$

$$h_n^{(2)} = j_n(x) - iy_n(x). \tag{A6}$$

The spherical Hankel function of the 2nd type with an order increase up to $n + 1/2$ can be written with respect to the cylindrical Hankel function as [73]

$$h_n^{(2)}(x) = \sqrt{\frac{\pi}{2x}} H^{(2)}_{n+\frac{1}{2}}(x). \tag{A7}$$

Using the expressions (A1)–(A4) and(A7), $Z_0$, $Z_{in}$ and $|S_{11}|$ (Figure A1) of the conic AE from Figure 8 *a* are calculated in the Octave mathematical package using the built-in implementations of calculating the cylindrical Hankel functions of the 2nd type and the Legendre polynomial. The geometric parameters of the AE were chosen similarly to those given in [58] at $\Theta_0 = 53{,}1°$.

The normalized radiation pattern of the conical AE is calculated as [58]

$$R(\theta) = \frac{E_\theta(r,\theta)}{E_\theta\left(r,\frac{\pi}{2}\right)} = \frac{\sum_{n=1}^{\infty} P_n(\cos(\Theta_0)) P_n^1(\cos(\theta)) \frac{2n+1}{n(n+1)} i^n \left[\frac{\zeta(ka)}{h_n^{(2)}(ka)}\right]}{\sum_{n=1}^{\infty} P_n(\cos(\Theta_0)) P_n^1(\cos(0)) \frac{2n+1}{n(n+1)} i^n \left[\frac{\zeta(ka)}{h_n^{(2)}(ka)}\right]}. \tag{A8}$$

Preprints (www.preprints.org) | NOT PEER-REVIEWED | Posted: 6 June 2022 doi:10.20944/preprints202206.0061.v1



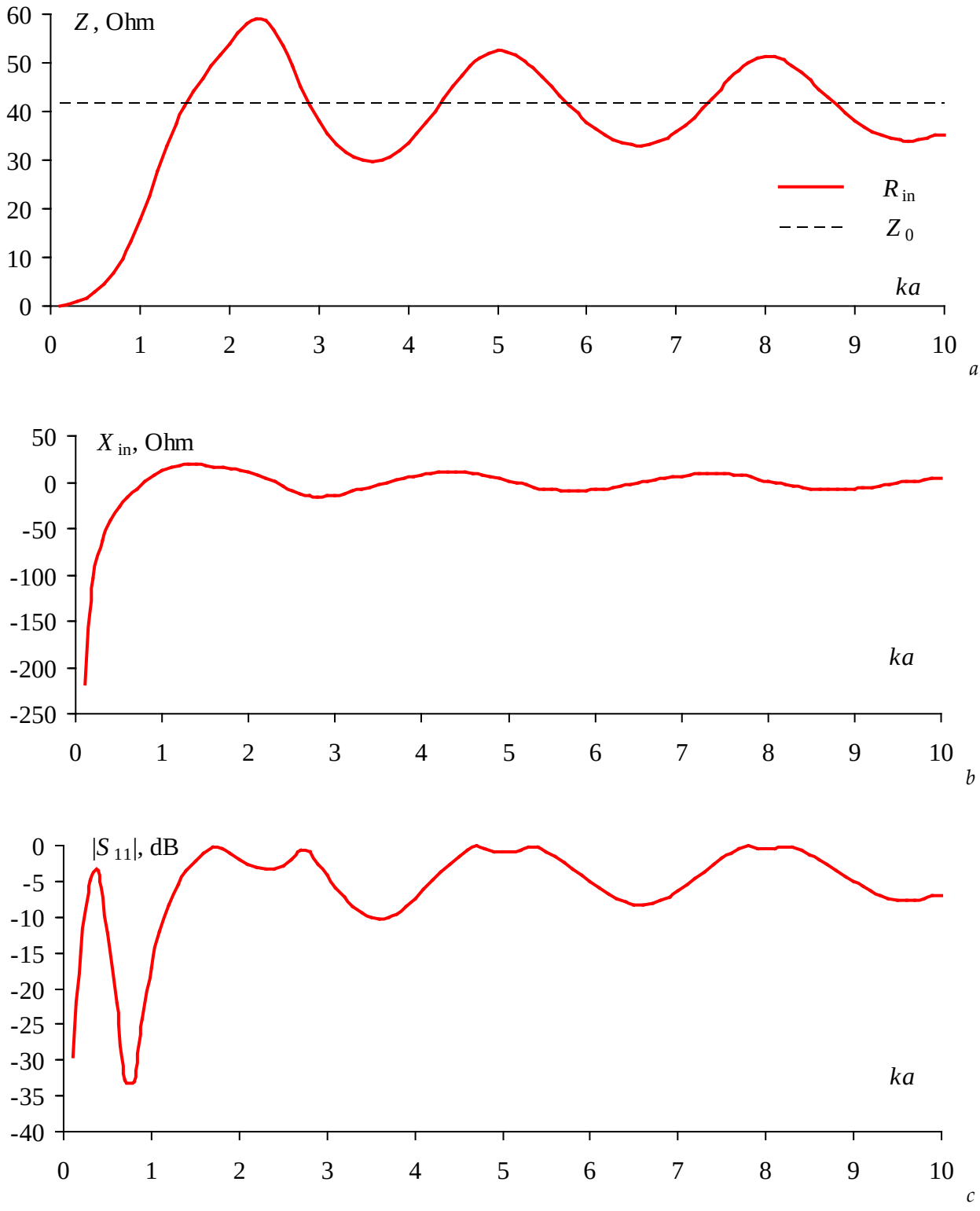


Figure A1. The dependences on *ka* of: characteristic impedance $Z_0$, the real $R_{in}$ and the imaginary $X_{in}$ parts of the input impedance $Z_{in}$, as well as $|S_{11}|$ for the conical AE from Figure 8*a* with $\Theta_0 = 53{,}1°$

In [59], the problem of estimating the emission and reception of electromagnetic waves for electrically small and large biconical AE having unequal angles of two cones is considered (Figure 8 *b*). Both cones are symmetrically excited at the vertices by a voltage source. To calculate the normalized RP of such AE, the following expression is used

Preprints (www.preprints.org) | NOT PEER-REVIEWED | Posted: 6 June 2022 doi:10.20944/preprints202206.0061.v1



$$R(\theta)=\frac{E_\theta(r,\theta)}{E_\theta\left(r,\frac{\pi}{2}\right)}=\frac{\sum_{n=1}^{\infty}\frac{i^{n-1}(2n+1)}{2n(n+1)}\frac{P_n^1(\cos(\theta))\left[P_n(\cos(\Theta_1))-(-1)^nP_n(\cos(\Theta_2))\right]}{h_{n-1}^{(2)}(ka)-\frac{n}{ka}h_n^{(2)}(ka)}}{\sum_{n=1}^{\infty}\frac{i^{n-1}(2n+1)}{2n(n+1)}\frac{P_n^1(0)\left[P_n(\cos(\Theta_1))-(-1)^nP_n(\cos(\Theta_2))\right]}{h_{n-1}^{(2)}(ka)-\frac{n}{ka}h_n^{(2)}(ka)}} \quad \text{(A9)}$$

where the Legendre function can be calculated as

$$P_n^1(\cos(\theta))=-\frac{d}{d\theta}P_n(\cos(\theta))=\frac{n}{\sin(\theta)}\left[P_{n-1}(\cos(\theta))-\cos(\theta)P_n(\cos(\theta))\right]. \quad \text{(A10)}$$

The input impedance of the biconical AE ($Z_{inB}$) is related to the impedance of the conical AE as [74]

$$Z_{inB}=2Z_{in}. \quad \text{(A11)}$$

The normalized RP of the biconical AE are calculated according to (A8) and (A9) at $a$ = 20' or 508 mm, with the opening angles of the cones $\Theta_1=\Theta_2=53{,}1°$, as well as $ka_1$ = 1,0640 ($f_1$ = 0,1 GHz) – Figure A2, $ka_2$=5,3198 ($f_2$ = 0,5 GHz) and $ka_3$ = 10,6395 ($f_3$ = 1 GHz) – Figure A3. The figures also show similar digitized values from [59].

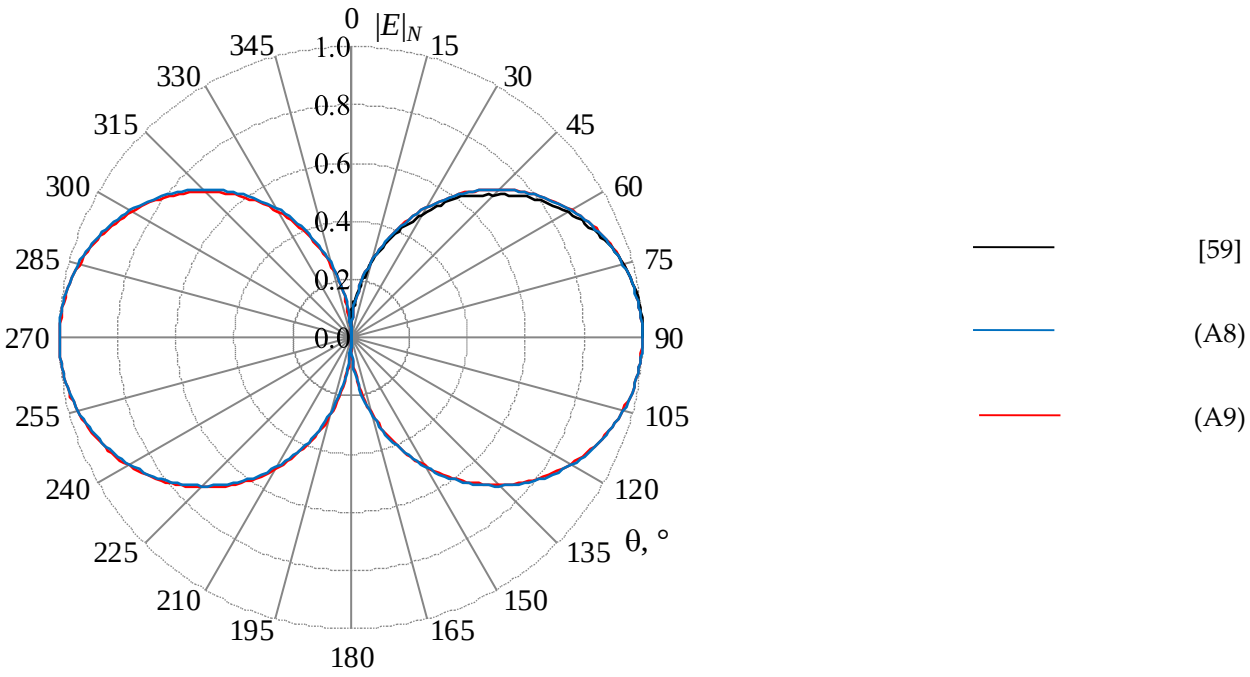


Figure A2. The normalized RP ($|E|_N$, times) of the biconical AE with $a$ = 508 mm and $\Theta_1=\Theta_2=53{,}1°$ with $ka_1$ = 1,0640 ($f_1$ = 0,1 GHz), calculated analytically

Preprints (www.preprints.org) | NOT PEER-REVIEWED | Posted: 6 June 2022 doi:10.20944/preprints202206.0061.v1



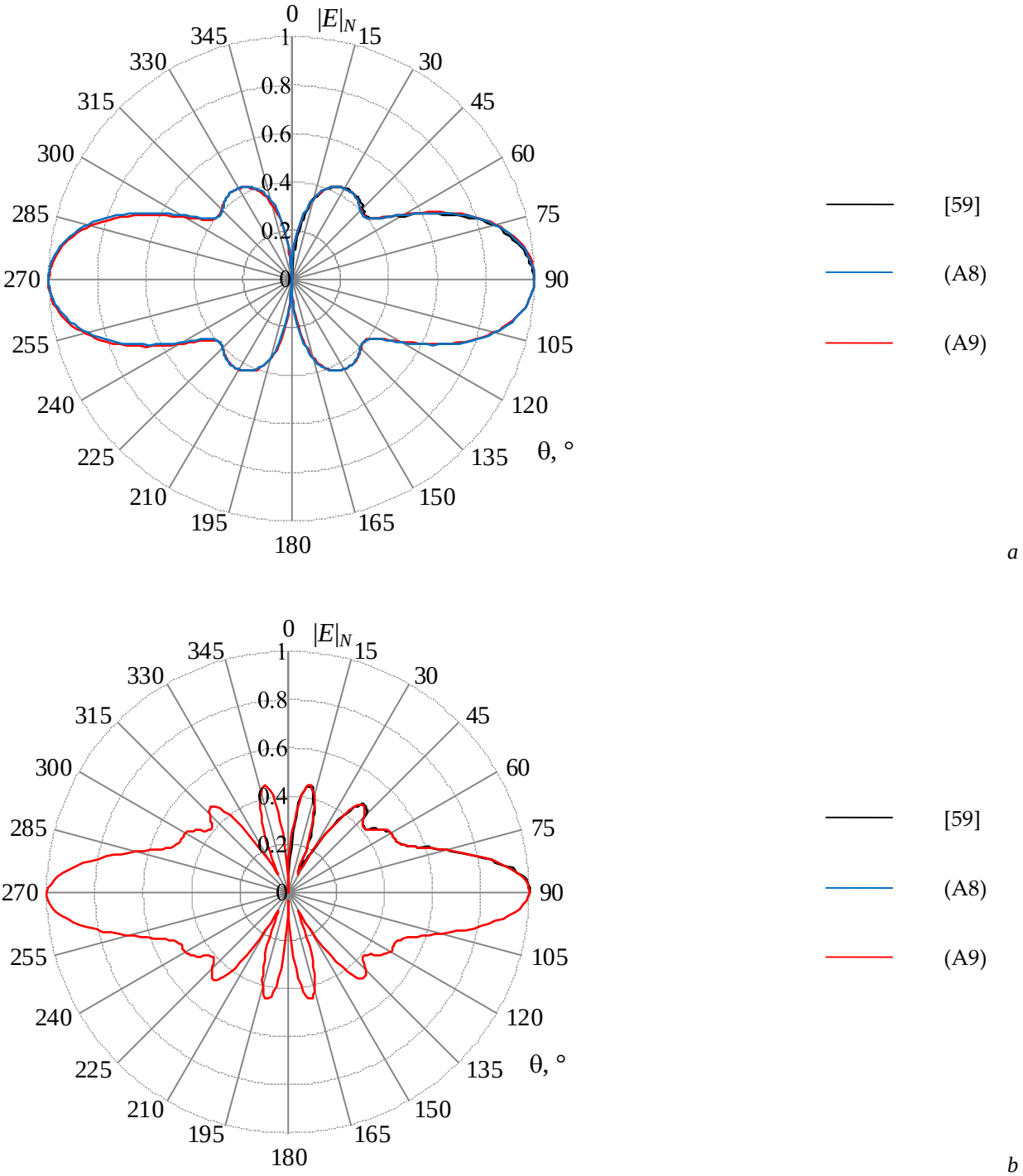


Figure A3. The normalized RP ($|E|_N$, times) of the biconical AE with $a$ = 508 mm and $\Theta_1 = \Theta_2 = 53{,}1°$ with $ka_2 = 5{,}3198$ ($f_2 = 0{,}5$ GHz) (*a*) and $ka_3 = 10{,}6395$ ($f_3 = 1$ GHz) (*b*), calculated analytically

Figures A2 and A3 show that the digitized data from [59] and those obtained from (A8) and (A9) almost completely coincide, which confirms the correctness of the software implementation of analytical models. At the same time, the normalized RPs from [59] were obtained at the specified values of $ka$, taking into account that the speed of light in vacuum was assumed to be equal to $3 \cdot 10^8$ m/s. However, modern CAD systems use its more accurate value of 299792448 m/s. Therefore, this difference, among other things, can have an effect on the resulting RP, and above all, at higher frequencies.

 doi:10.20944/preprints202206.0061.v1



## Appendix B

Here, the gain values of the horn AE from Section 3.3 calculated at the frequency of 8 GHz with the nominal parameters presented in Table 7 modeled using the settings summarized in Table 8 are shown in Figures B1–B4. It can be seen that the values converge with using $L_e = 16$ and increasing $L_r$. So, the transition from $L_r = 2$ to $L_r = 4$ leads to a maximum change in gain value, and the transition from $L_r = 8$ to $L_r = 16$ leads to a minimum change. As can be seen from Figures B4 and B3, the gain values at a fixed value of $L_r$ and an increase in $n$ converge well. Therefore, the values $n = 40$ and $L_r = 8$ seem to be the minimum optimal values for modeling such AEs and therefore they were used in the further calculations in Section 3.3.

Preprints (www.preprints.org) | NOT PEER-REVIEWED | Posted: 6 June 2022 doi:10.20944/preprints202206.0061.v1



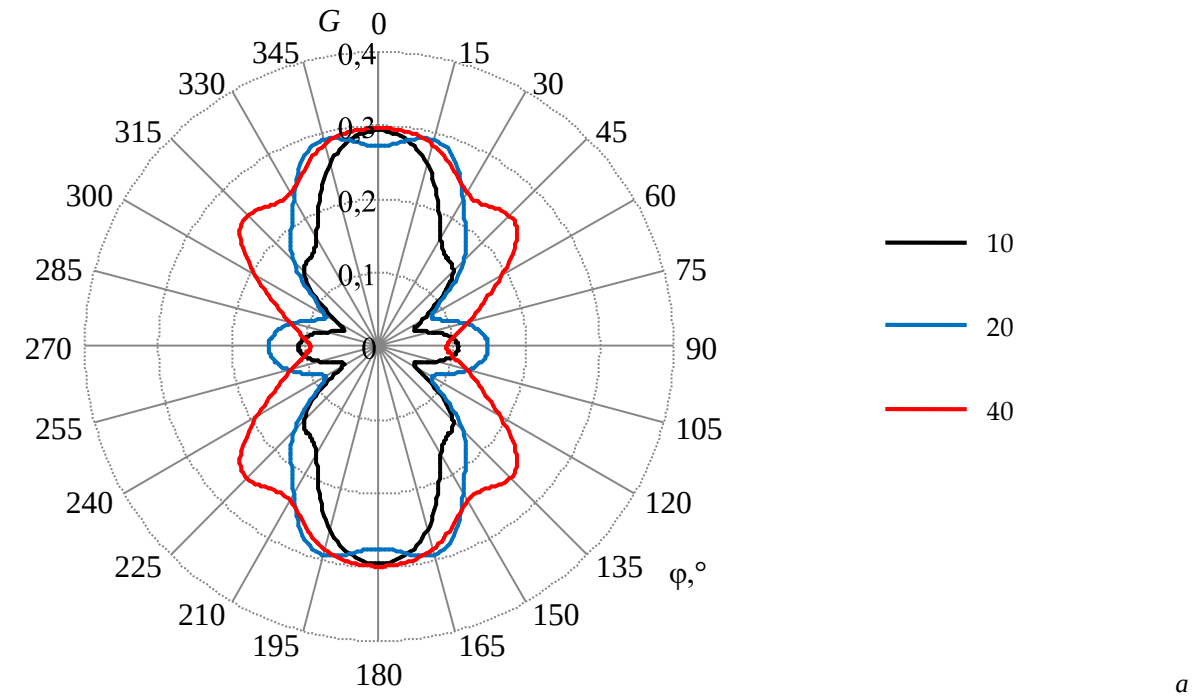


*a*

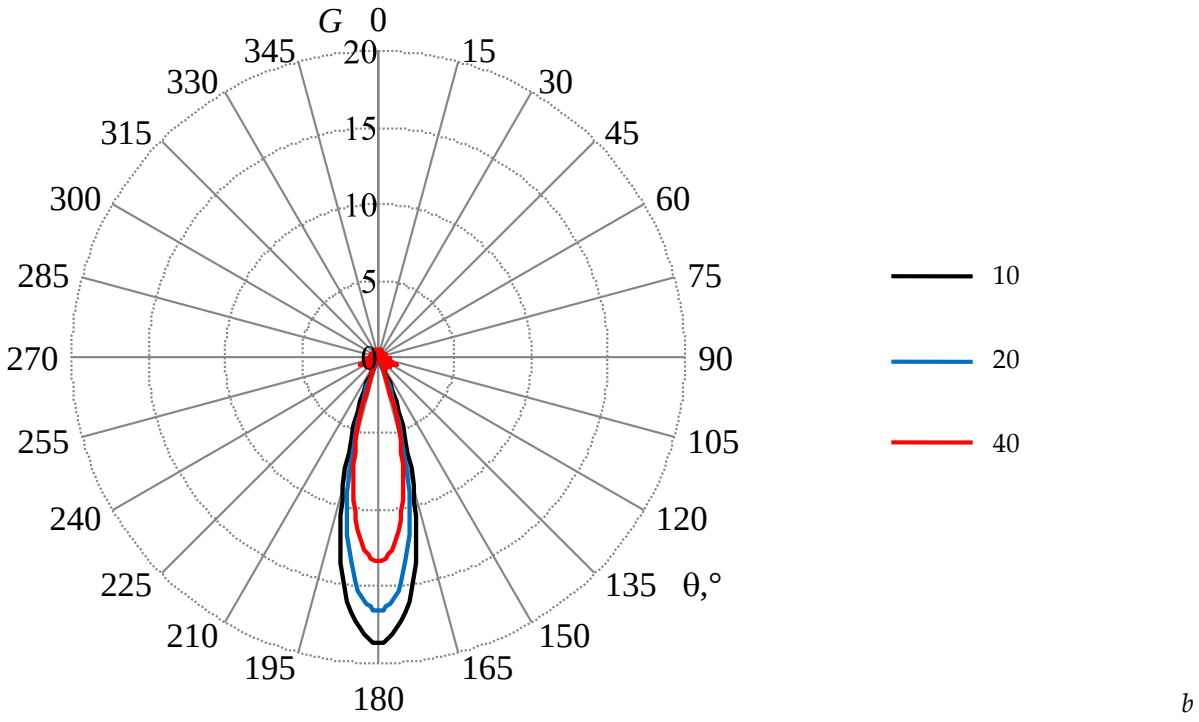


*b*

Figure B1. The gain (*G*, times) of the horn AE at the frequency of 8 GHZ
in θ = 90° (*a*) and φ = 90°planes (*b*), calculated in the wire-grid, with $L_r$ = 2 and $n$ = 10, 20, and 40

Preprints (www.preprints.org) | NOT PEER-REVIEWED | Posted: 6 June 2022 doi:10.20944/preprints202206.0061.v1



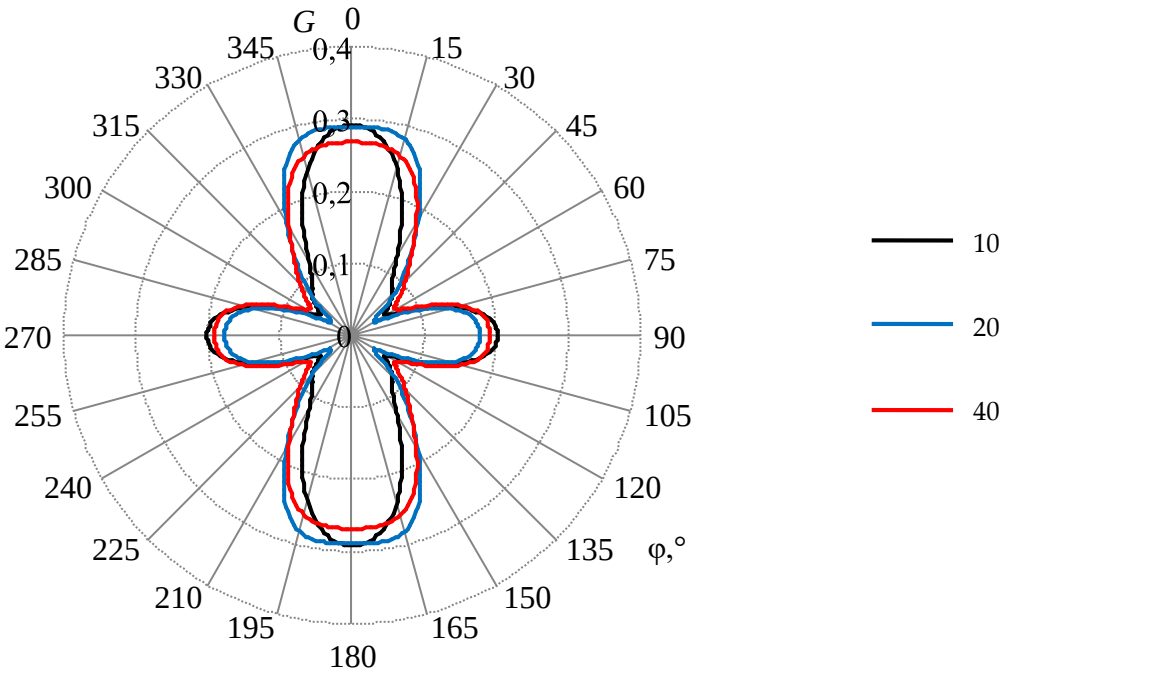


*a*

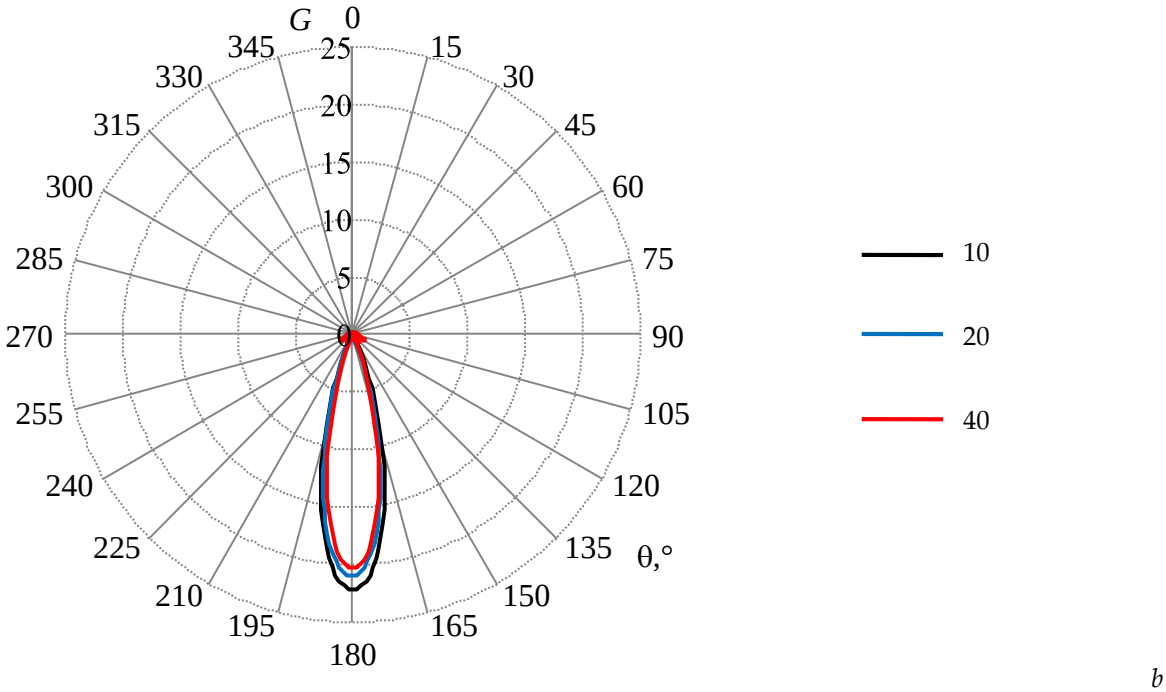


*b*

Figure B2. The gain (*G*, times) of the horn AE at the frequency of 8 GHZ in θ = 90° (*a*) and φ = 90°planes (*b*), calculated in the wire-grid, with $L_r$ = 4 and *n* = 10, 20, and 40

Preprints (www.preprints.org) | NOT PEER-REVIEWED | Posted: 6 June 2022 doi:10.20944/preprints202206.0061.v1



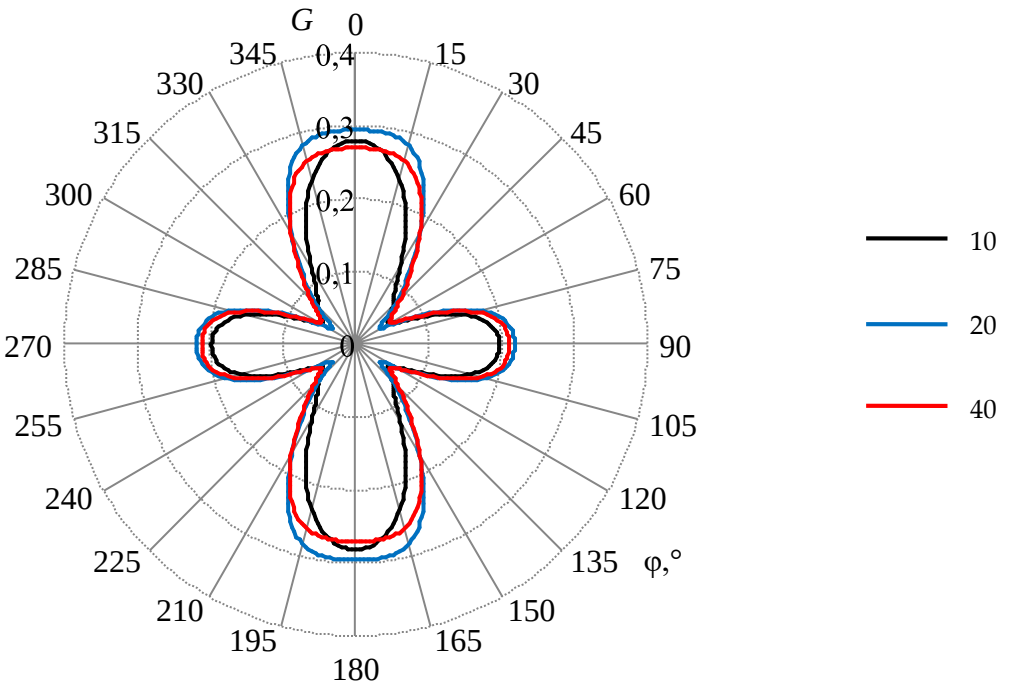


*a*

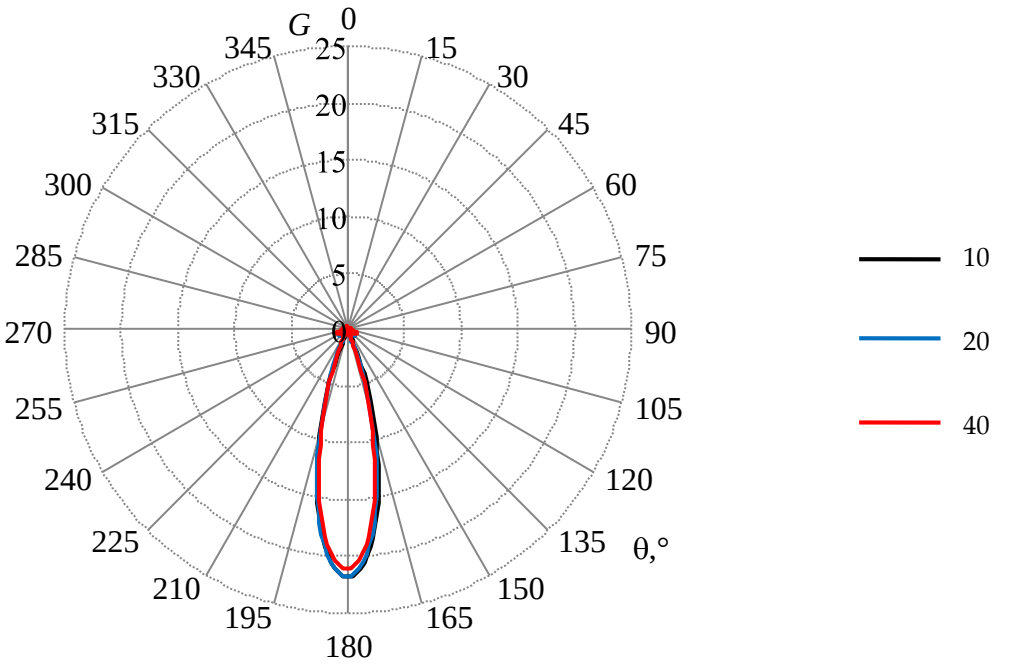


*b*

Figure B3. The gain (*G*, times) of the horn AE at the frequency of 8 GHZ in θ = 90° (*a*) and φ = 90°planes (*b*), calculated in the wire-grid, with $L_r$ = 8 and *n* = 10, 20 and 40

Preprints (www.preprints.org) | NOT PEER-REVIEWED | Posted: 6 June 2022 doi:10.20944/preprints202206.0061.v1



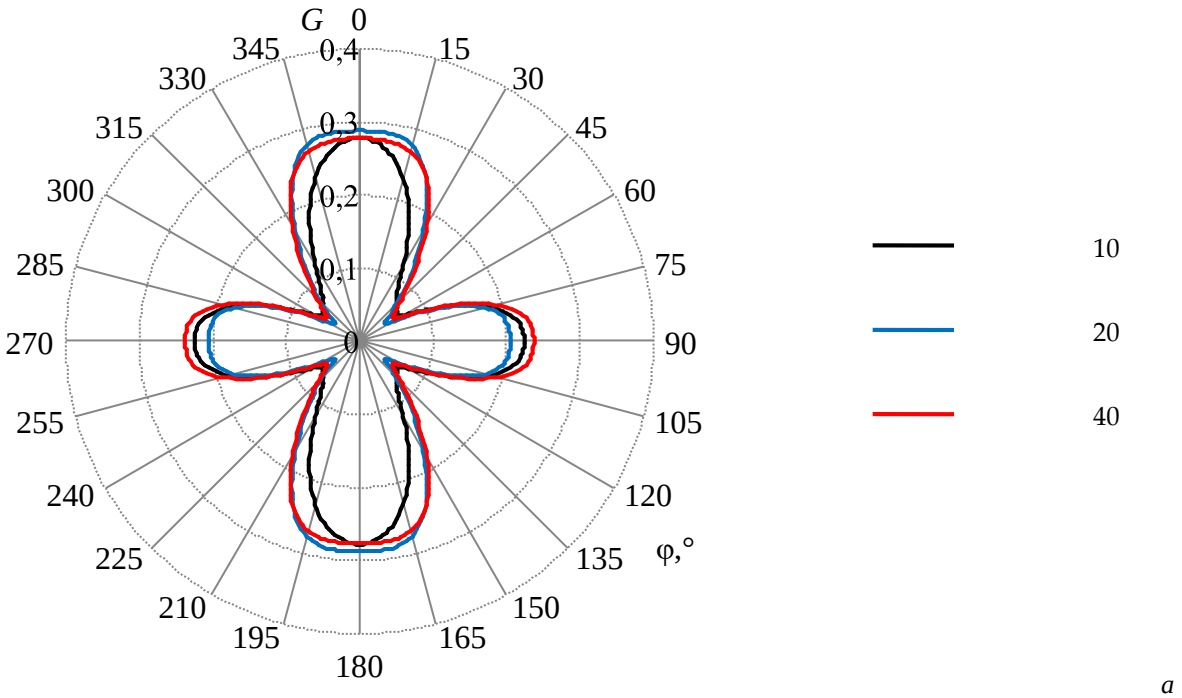


*a*

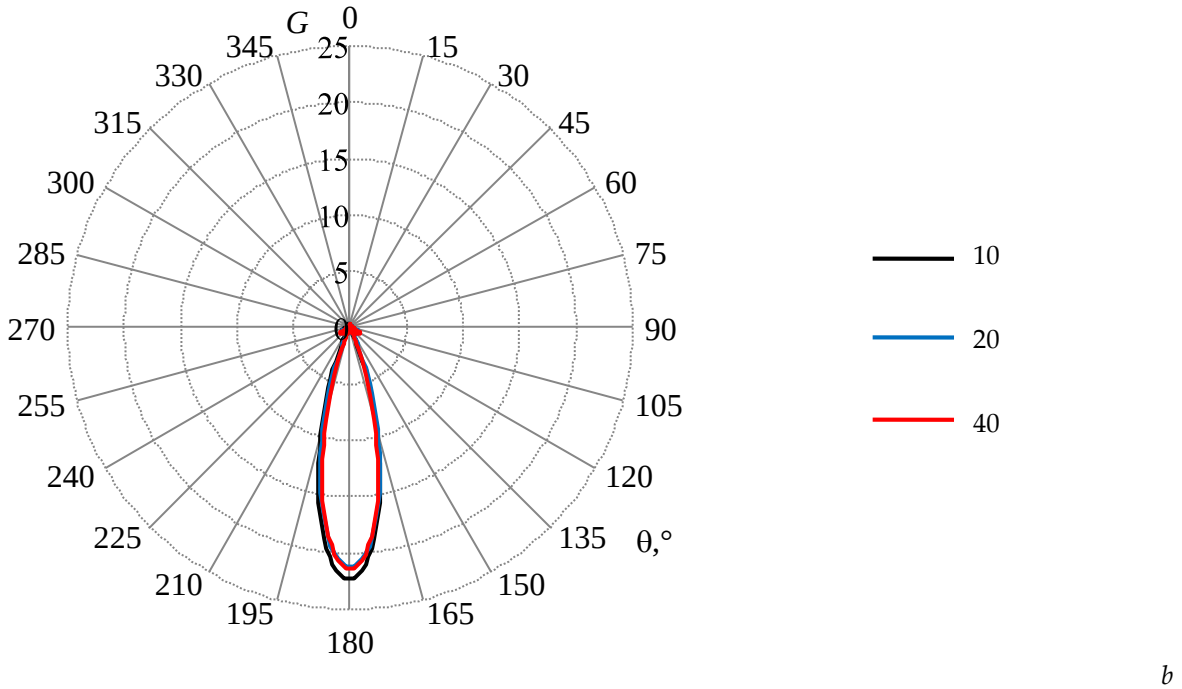


*b*

Figure B4. The gain (*G*, times) of the horn AE at the frequency of 8 GHZ
in θ = 90° (*a*) and φ = 90°planes (*b*), calculated in the wire-grid, with $L_r$ = 16 and $n$ = 10, 20 and 40

## References


1. Grigorev, A.D. *Metody vychislitelnoi elektrodinamiki*; Fizmatlit: Moscow, Russia, **2013**; p. 430. (In Russian)
2. Il'in, V.P. Matematicheskoe modelirovanie i filosofiya nauki. *Vestnik Rossiiskoi akademii nauk* **2018**, *88*, 58–66. (In Russian)
3. Yee, K.S. Numerical solution of initial boundary value problems involving Maxwell's equations in esotropic media. *IEEE Trans. on antennas and propagation* **1966**, *14*, 302–307. DOI: 10.1109/TAP.1966.1138693.
4. Taflove, A. Application of the finite-difference time-domain method to sinusoidal steady state electromagnetic penetration problems. *IEEE Trans. on electromagn. comp.* **1980**, *22*, 191–202. DOI: 10.1109/TEMC.1980.303879.
5. Weiland, T. A discretization method for the solution of Maxwell's equations for six-component fields. *Electronics and communications AEUE* **1977**, *31*, 116–120.
6. Clemson vehicular electronics laboratory. Available online: cecas.clemson.edu/cvel/modeling/tutorials/techniques/fit/finite_integration.html (accessed on 19.03.2022).
7. Courant, R. Variational methods for the solution of problems of equilibrium and vibrations. *Bulletin of American mathematical society* **1943**, *49*, 1–23. DOI: 10.1090/S0002-9904-1943-07818-4.
8. Rao, S; Wilton, D; Glisson, A. Electromagnetic scattering by surfaces of arbitrary shape. *IEEE Transactions on antennas and propagation* **1982**, *30*, 409–418. DOI: 10.1109/TAP.1982.1142818.
9. Pocklington, H.C. Electrical oscillations in wires. *Mathematical proceedings of the Cambridge philosophical society* **1897**, 324–332.
10. Hallen, E. Theoretical investigation into the transmitting and receiving qualities of antennas. *Nova Acta (Uppsala)* **1938**, 1–44.
11. Levin, B.M. *The theory of thin antennas and its use in antenna engineering*; Bentham Science Publ, 2013; p. 318. DOI: 10.2174/97816080577331130101.
12. King, R.W.P.; Smith, G.S.; Owens, M.; Wu, T.T. *Antennas in matter: Fundamentals, theory, and applications*; Cambridge, Mass.:MIT Press, 1981; p. 880.
13. Richmond, J.H. Digital computer solution of the rigorous equations for scattering problems. *Proc. of the IEEE* **1965**, *53*, 796–804. DOI: 10.1109/PROC.1965.4057.
14. Nazarov, V.E.; Runov, A.V.; Podininogin V.E. Chislennoe reshenie zadach ob osnovnyh harakteristikah i parametrah slozhnyh provolochnyh antenn. *Radiotekhnika i elektronika* **1976**, 153–157. (In Russian)
15. Strizhkov, V.A. Matematicheskoe modelirovanie elektricheskih processov v provolochnyh antennyh sistemah. *Matematicheskoe modelirovanie* **1989**, *1*, 127–138. (In Russian)
16. Eminov, S.I. Teoriya integral'nogo uravneniya tonkogo vibratora. *Radiotekhnika i elektronika* **1993**, *38*, 2160–2168. (In Russian)
17. Werner, D.H.; Werner, P.L.; Breakall, J.K. Some computational aspects of Pocklington electric field integral equation for thin wires. *IEEE Transactions on antennas and propagation* **1994**, *42*, 561–563. DOI: 10.1109/8.286230.
18. Kraus, J.D.; Marhefka, R.J. *Antennas for all applications*; New Delhi: McGraw-Hill, 2006; p. 892.
19. Richmond, J.H. A wire-grid model for scattering by conducting bodies. *IEEE Trans. on antennas and propagation* **1966**, *AP-14*, 782–786. DOI: 10.1109/TAP.1966.1138783.
20. Numerical Electromagnics Code (Method of Moments). NEC simulates the electromagnetic response of antennas and metal structures. Available online: nec2.org (accessed on 19.03.2022).
21. Gee, S.; Miller, E.K.; Poggio, A.J.; et al. Computer techniques for electromagnetic scattering and radiation analyses. *Comp. Electromagnetics. Frequency Domain Method of Moments* **1992**, 142–152. DOI: 10.1109/ISEMC.1971.7567924.
22. Stutzman, W.L.; Thiele, G.A. *Antenna theory and design*; John Wiley & Sons, 2001; p. 598.
23. Lee K.S.H.; Marin, L.; Castillo P. Limitations of Wire-Grid Modeling of a Closed Surface. *IEEE Transactions on electromagnetic compatibility* **1976**, 18, 123–129. DOI: 10.1109/TEMC.1976.303482.
24. Rubinstein, A.; Rachidi, F.; Rubinstein, M. A Parallel Implementation of NEC for the analysis of large structures. *IEEE Transactions on electromagnetic compatibility* **2003**, 45, 177–188. DOI: 10.1109/TEMC.2003.810806.
25. Joy, V.; Rajeshwari, G.L.; Singh, H.; Nair, R.U. *Fundamentals of RCS prediction methodology using parallelized Numerical Electromagnetics Code (NEC) and finite element pre-processor*; Springer: Singapore, 2021. DOI: 10.1007/978-981-15-7164-0_4.
26. Rubinstein, A.; Rachidi, F.; Rubinstein M. On wire-grid representation of solid metallic surfaces. *IEEE Transactions on electromagnetic compatibility* **2005**, 47, 192–195. DOI: 10.1109/TEMC.2004.838230.
27. Topa, T.; Karwowski, A.; Noga A. Using GPU with CUDA to accelerate MoM-based electromagnetic simulation of wire-grid models. *IEEE Antennas wireless and propagation letters* **2011**, 10, 342–345. DOI: 10.1109/LAWP.2011.2144557.
28. Burke, G.; Poggio, A. *Numerical electromagnetics code - method of moments*; Lawrence Livermore National Laboratory: Livermore, USA, 1981.
29. Werner, D.H. A method of moments approach for the efficient and accurate modeling of moderately thick cylindrical wire antenna. *IEEE Transactions on antennas and propagation* **1998**, 46, 373–382. DOI: 10.1109/8.662656.
30. CONCEPT-II Version 12.0 user's manual. Available online: URL: https://www.tet.tuhh.de/concept-II-12.0/Concept-II-Manual-December-2018.pdf (accessed on: 19.03.2022).
31. Trueman, C.W.; Kubina, S.J. Fields of complex surfaces using wire grid modeling. *IEEE Transactions on magnetic* **1991,** 27, 4262–4267. DOI: 10.1109/20.105043.
32. Garcia, S.G.; Martin, R.G.; Pantoja M.F. On the simulation of a GPR using an ADI-FDTD MoMTD hybrid method. *Proceedings of the tenth international conference on ground penetrating radar* **2004**, 1, 13–15.

33. Jiangdong, L.; Zhen, T.; Feng, X. An FDTD/MoMTD hybrid technique for modeling HF antennas located on lossy ground. *International conference on microwave and millimeter wave technology* **2008**, 2, 726–729. DOI: 10.1109/ICMMT.2008.4540498.
34. Karwowski, A.; Noga, A. Fast MM-PO-based numerical modeling technique for wideband analysis of antennas near conducting objects. *Electronics letters* **2007**, 43, 486–487. DOI: 10.1049/el:20070557.
35. Bingle, M.; Burger, W.; Ludick, D. Method of moments accelerations and extensions in FEKO. *International conference on electromagnetics in advanced applications (ICEAA)* **2011**, 62–65. DOI: 10.1109/ICEAA.2011.6046328.
36. Fujiwara, O.; Jianqing, W.; Wake, K. A hybrid MoM/FDTD method for dosimetry of small animal in reverberation chamber. *IEEE Transactions on electromagnetic compatibility* **2014**, 56, 549–558. DOI: 10.1109/TEMC.2014.2304958.
37. Kojima, M.; Sasaki, K.; Suzuki, Y.M. Analysis of millimeter-wave exposure on rabbit eye using a hybrid PMCHWT-MoM-FDTD method. *The International symposium on antennas & propagation* **2013**, 1, 59–62. DOI: 10.34385/proc.54.WP-1(B)-4.
38. Karwowski, A.; Noga, A. Wide-band hybrid MM-PO computational electromagnetics technique using [Z] matrix interpolation and adaptive frequency sampling. *IEEE International symposium on electromagnetic compatibility* **2007**, 1–4. DOI: 10.1109/ISEMC.2007.111.
39. Commens, M.; Zhao, K. Efficient large-scale simulations with a hybrid finite element boundary integral technique. *IEEE 13th annual wireless and microwave technology conference (WAMICON)* **2012**, 1–4. DOI: 10.1109/WAMICON.2012.6208447.
40. Sadiku, M.N.O. *Numerical techniques in electromagnetics*, 3rd ed; CRC Press: Boca Raton, USA, 2009. DOI: 10.1201/9781420058277.
41. Dworsky, N. *Introduction to numerical electrostatics using MATLAB*; John Wiley & Sons: Hoboken, USA, 2014. DOI: 10.1002/9781118758571.
42. Poljak, D. *Advanced modeling in computational electromagnetic compatibility*; John Wiley & Sons: Hoboken, USA, 2007. DOI: 10.1002/0470116889.
43. Sevgi, L. *Electromagnetic modeling and simulation*; John Wiley & Sons: Hoboken, USA, 2014. DOI:10.1002/9781118716410.
44. Tarasik, V.P. *Matematicheskoe modelirovanie tekhnicheskih sistem: uchebnik dlya vuzov*; Dizajn PRO: Moscow, Russia, 2004. (In Russian).
45. Liu, Y.; Hu, J.; Mei, K.K. A novel fast iteration technique for scattering by 2-D perfect conducting cylinders. *IEEE Transactions electromagnetic compatibility* **2002**, 44, 263–265. DOI: 0.1109/15.990734.
46. Davidson, D.B. *Computational electromagnetics for RF and microwave engineering*; University Press: Cambridge, England, 2011. DOI: 10.1017/CBO9780511778117.
47. Gibson, W.C. *The method of moments in electromagnetic*; Chapman & Hall/CRC: Boca Raton, USA, 2008. DOI: 10.1201/9780429355509.
48. Makarov, S.N. *Antenna and EM modeling with MATLAB*; John Wiley & Sons: New York, USA, 2002.
49. Peterson, A.F.; Ray, S.L.; Mittra, R. Computational methods for electromagnetics; Wiley and IEEE Press, 1998; p. 592.
50. Mittra, R. Computer techniques for electromagnetics: international series of monographs in electrical engineering; Pergamon Press and Elsevier, 2013; p. 416.
51. Harrington, R.F. *Field computation by moment methods*; Macmillan: New York, USA, 1968. DOI: 10.1093/comjnl/12.1.37.
52. Crandall, S.H. *Engineering analysis*; McGraw-Hill: New York, USA, 1956.
53. Ludwig, C. Wire grid modeling of surfaces. *IEEE Transactions on antennas and propagation* **1987**, AP-35, 1045–1048. DOI: 10.1109/TAP.1987.1144220.
54. Mayhan, J.T. Characteristic modes and wire grid modeling. *IEEE Transactions on antennas and propagation* **1990**, 38, 457–469. DOI: 10.1109/8.52263.
55. Rubinstein, A.; Rubinstein, M.; Rachidi, F. A physical interpretation of the equal area rule. *IEEE Transactions on electromagnetic compatibility* **2006**, 48, 258–263. DOI: 10.1109/TEMC.2006.873861.
56. EMPro system. Available online: keysight.com/ru/ru/products/software/pathwave-design-software/pathwave-em-design-software.html (accessed on 19.03.2022).
57. Papas, C.H.; King, R. Input impedance of wide-angle conical antennas fed by a coaxial line. *Proceedings of the IRE* **1949**, 37, 1269–1271. DOI: 10.1109/JRPROC.1949.234607.
58. Papas, C.H.; King, R. Radiation from wide-angle conical antennas fed by a coaxial line. *Proceedings of the IRE* **1951**, 39, 49–51. DOI: 10.1109/JRPROC.1951.230420.
59. Samaddar, S.N.; Mokole, E.L. Biconical antennas with unequal cone angles. *IEEE Transactions on antennas and propagation* **1998**, 181–193. DOI: 10.1109/8.660962.
60. Golub, G. H., Van Loan, C. F. *Matrix computation*; The Johns Hopkins University Press, 1996; p. 723.
61. Higham, N.J. *Accuracy and stability of numerical algorithms*. Philadelphia: SIAM, 2002; p. 680.
62. Sarkar, T.K., Siarkiewicz, K., Stratton, R. Survey of numerical methods for solution of large systems of linear equations for electromagnetic field problems. *IEEE Transactions on antennas and propagation* **1981**, Vol. 29, pp. 847–856. DOI: 10.1109/TAP.1981.1142695.
63. Verzhbickij, V.M. *Osnovy chislennyh metodov*; Vysshaya shkola: Moscow, Russia, 2002; p. 840. (In Russian).
64. Balanis, C. A. *Modern Antenna Handbook*; 2008; pp. 1461–1494. DOI: 10.1002/9780470294154.
65. Mittra, R. *Computational electromagnetics: recent advances and engineering applications*; New York: Springer Science+Business Media, 2014; p. 707. DOI: 10.1007/978-1-4614-4382-7.
66. Olyslager, F., Lermans, E., de Zutter D. Numerical and experimental study of the shielding effectiveness of a metallic enclosure. *IEEE Transactions on electromagnetic compatibility* **1999**, Vol. 41, no. 3., pp. 202–213. DOI: 10.1109/15.784155.

67. Correira, L.M. A comparison of integral equation with unique solution in the resonance region for scattering by conducting bodies. *IEEE Transactions on antennas and propagation* **1993**, Vol. 41, no. 1., pp. 52–58. DOI: 10.1109/8.210115.
68. Ji Y., Hubing T. H. On the interior resonance problem when applying a hybrid FEM/MoM approach to model printed circuit boards. *IEEE Transactions on electromagnetic compatibility* **2002**, Vol. 44, no. 2. pp. 318–323. DOI: 10.1109/TEMC.2002.1003396.
69. Sheng, X. Q., Jin, J. M., Song, J., et al. On the formulation of hybrid finite–element and boundary–integral methods for 3-D scattering. *IEEE Transactions on antennas and propagation* **1998**, Vol. 46, no. 3. pp. 303–311. DOI: 10.1109/8.662648.
70. Nayanthara, K., Rao, S., Sarkar, T. Analysis of two–dimensional conducting and dielectric bodies utilizing the conjugate gradient method. *IEEE Transactions on antennas and propagation* **1987**, Vol. 35, no. 4. pp. 451–453. DOI: 10.1109/TAP.1987.1144123.
71. Heath M. T. *Scientific computing: an introductory survey*; Boston: McGraw-Hill, 2018, p. 568. DOI: 10.2514/1.J060261.
72. Kuksenko, S.P.; Gazizov, T.R. *Iteracionnye metody resheniya sistemy linejnyh algebraicheskih uravnenij s plotnoj matricej*; Tomskij gosudarstvennyj universitet: Tomsk, Russia, 2007; p. 208. (In Russian).
73. Degauque, P.; Fontaine, J.; Gabillard, R. Theory of a thin biconical antenna located near the air-ground interface. *IEEE Transactions on antennas and propagation* **1975**, 420–424. DOI: 10.1109/TAP.1975.1141082.
74. Balanis, C.A. *Antenna theory: analysis and design*, 3rd ed.; John Wiley & Sons: New York, USA, 2005.